Cloud Phase Simulation at High Latitudes in EAMv2: Evaluation using CALIPSO Observations and Comparison with EAMv1

Meng Zhang[1], Shaocheng Xie[1], Xiaohong Liu[2], Wuyin Lin[3], Xue Zheng[1], Jean-Christophe Golaz[1], Yuying Zhang[1]

[1] Lawrence Livermore National Laboratory, Livermore, CA, USA

[2] Department of Atmospheric Sciences, Texas A&M University, College Station, TX, USA

[3] Brookhaven National Laboratory, Upton, NY, USA

Corresponding author: Meng Zhang, zhang55@llnl.gov

Key Points:

- EAMv2 substantially improves cloud ice phase at high latitude regions, while biases in liquid phase shown in EAMv1 remain.
- Updated tuning parameters in WBF process and deep convection are important for reduced negative bias in ice phase clouds.
- The new dCAPE_ULL trigger in deep convection is largely responsible for the better cloud phase simulation over high-latitude oceans.

Abstract

This study performs a comprehensive evaluation of the simulated cloud phase in the U.S. Department of Energy (DOE) Energy Exascale Earth System Model (E3SM) atmosphere model version 2 (EAMv2) and version 1 (EAMv1). Enabled by the CALIPSO (Cloud-Aerosol Lidar and Infrared Pathfinder Satellite Observation) simulator, EAMv2 and EAMv1 predicted cloud phase is compared against the GCM-Oriented CALIPSO Cloud Product (CALIPSO-GOCCP) at high latitudes where mixed-phase clouds are prevalent. Our results indicate that the underestimation of cloud ice in simulated high-latitude mixed-phase clouds in EAMv1 has been significantly reduced in EAMv2. The increased ice clouds in the Arctic mainly result from the modification on the WBF (Wegner-Bergeron-Findeisen) process in EAMv2. The impact of the modified WBF process is moderately compensated by the low limit of cloud droplet number concentration (CDNC) in cloud microphysics and the new dCAPE_ULL trigger used in deep convection in EAMv2. Moreover, it is found that the new trigger largely contributes to the better cloud phase simulation over the Norwegian Sea and Barents Sea in the Arctic and the Southern Ocean where large errors are found in EAMv1. However, errors in simulated cloud phase in EAMv1, such as the overestimation of supercooled liquid clouds near the surface in both hemispheres and the underestimation of ice clouds over Antarctica, persist in EAMv2. This study highlights the impact of deep convection parameterizations, which has not been paid much attention, on high-latitude mixed-phase clouds, and the importance of continuous improvement of cloud microphysics in climate models for accurately representing mixed-phase clouds.

1. Introduction

Clouds play an essential role in global climate through interactions with radiation and hydrological cycle. The extensive coverage and strong radiative effects make clouds an important modulator of the energy budget at the surface and top of the atmosphere (TOA). Cloud radiative effects are controlled by cloud optical depth and other optical properties that are closely related to cloud microphysical properties such as amount, size, shape, and thermodynamic phase of cloud hydrometeors (Curry et al., 1996; Curry & Ebert, 1992; Shupe & Intrieri, 2004). Compared to the sensitivity to cloud ice water, cloud albedo tends to be more sensitive to variations in cloud liquid water. The shortwave radiative cooling effect due to liquid water usually dominates the net cloud radiative effect in mixed-phase clouds, highlighting the importance of cloud thermodynamic phase on cloud radiative forcing (Sun & Shine, 1994). In addition, differences in microphysical properties between liquid and ice are critical for global precipitation. Satellite observations have demonstrated that most of the Earth's precipitation originates from the ice phase and mixed-phase cloud processes, while warm rain mechanisms are more critical for precipitation over tropical and subtropical oceans (Field & Heymsfield, 2015; Heymsfield et al., 2020; Mülmenstädt et al., 2015). The distinct roles of cloud liquid and cloud ice on precipitation formation make cloud phase one of the key factors influencing the hydrological cycle in the Earth system. Moreover, the amount of cloud water in the liquid and ice phase in the present-day climate can also have a significant impact on the future climate (Bjordal et al., 2020; Lohmann & Neubauerm 2018; Tsushima et al., 2006). If clouds in the present-day climate have a lower ice water amount, the phase transition from ice to liquid would be less significant in the future warming climate, which would result in a weaker negative cloud phase feedback and thus a warmer future climate (Murray et al., 2021; Tan et al., 2016). Therefore, understanding processes controlling cloud phase is crucial to future climate change.

Mixed-phase clouds, composed of both liquid and ice, are frequently observed in high-latitude regions (Hu et al., 2010; McFarquhar et al., 2021; Shupe, 2011). In the Arctic, mixed-phase clouds were observed for up to ~40% of the time during the Surface Heat Budget of the Arctic Ocean (SHEBA) field campaign (Intrieri et al., 2002; Shupe et al., 2006). There are substantial seasonal variations in the occurrence of Arctic mixed-phase clouds. Both ground-based and spaceborne data suggest that the maximum frequency of occurrence of mixed-phase clouds typically occurs in the late summer and fall while the minimum is in winter (Cox et al., 2014; Shupe et al., 2011; D. Zhang et al., 2010). Although multi-layer clouds are also observed, single-layer stratiform mixed-phase clouds are one of the ubiquitous cloud types in the Arctic (Shupe et al., 2006). These single-layer stratiform mixed-phase clouds are usually located within the boundary layer, topped by a supercooled liquid layer from which ice particles are formed and precipitate (de Boer et al., 2009; Shupe et al., 2006, 2011). Temperature and moisture inversions are commonly found above or near the cloud top, which implies the importance of complicated interactions among radiation, large-scale advection, turbulence, cloud microphysics, and surface processes on promoting the persistent Arctic mixed-phase cloud system (Morrison et al., 2012; Sedlar et al., 2012).

The Southern Ocean (SO) and Antarctica are the other regions where mixed-phase clouds are commonly observed. Adhikari et al. (2012) used Cloud-Aerosol Lidar and Infrared Pathfinder Satellite Observation (CALIPSO) and CloudSat observations to study the seasonal and interannual variability of cloud distributions in the Antarctic. They showed that more than 60% of the total cloudiness were low-level clouds, and larger cloud occurrence was found during summer than winter. The large occurrence of low-level supercooled liquid clouds is also confirmed from the Measurements of Aerosols, Radiation and Clouds over the Southern Ocean (MARCUS) field campaign (McFarquhar et al., 2021). For instance, McFarquhar et al. (2021) found that cloud base temperature of over 49% of nonprecipitating clouds was below 0℃ over the SO. At McMurdo station on the Ross Island, data collected from the U.S. Department of Energy (DOE) Atmospheric Radiation Measurement (ARM) West Antarctic Radiation Experiment (AWARE) field campaign further suggested that cloud frequency of occurrence, cloud height, and cloud thickness of Antarctic clouds are quite different from those in the Arctic (Lubin et al., 2020; D. Zhang et al., 2019).

Cloud microphysical processes often occur at a scale smaller than a typical grid box used in global climate models (GCMs). They have to be parameterized in these models. Large uncertainties in numerical simulations of mixed-phase cloud properties are often associated with cloud microphysics parameterizations (Bodas-Salcedo et al., 2016; Forbes & Ahlgrimm, 2014; Morrison et al., 2020; Xie et al., 2008, 2013). For example, for GCMs that participated in the 5th phase of the Coupled Model Intercomparison Project (CMIP5), the temperature at which simulated mixed-phase clouds have equal amounts of liquid and ice was found to vary by 40℃ (McCoy et al., 2015). Such a sizeable inter-model spread is primarily caused by uncertainties in the representation of cloud microphysical processes in GCMs (McCoy et al., 2015, 2016). Furthermore, the equilibrium climate sensitivity (ECS) estimated from the 6th phase of the Coupled Model Intercomparison Project (CMIP6) models also vary significantly. The mean ECS has increased by 1.5℃ compared to that of CMIP5 models (Bodas-Salcedo et al., 2019; Gettelman et al., 2019; Zelinka et al., 2020). The changed model behavior in simulated cloud phase is one of the primary reasons for higher ECSs in many CMIP6 models (Bjordal et al., 2020; Lohmann & Neubauerm, 2018).

To better understand and quantify biases in modeled clouds, instrument simulators have been developed and incorporated in GCMs to enable consistent comparisons between model outputs and satellite observed cloud quantities. The Cloud Feedback Model Intercomparison Project (CFMIP) Observation Simulator Package (COSP) (Bodas-Salcedo et al., 2011; Swales et al., 2018) has been widely used in model evaluation studies (Cesana et al., 2012; Cesana & Chepfer, 2012; Kay et al., 2016; Y. Zhang et al., 2010, 2019). The advantage of COSP satellite simulators is that they can transfer grid-mean model quantities to quantities that satellites would directly measure from space. In addition, the simulated cloud horizontal subgrid distribution and vertical overlap are treated in the simulator to permit definition-consistent comparisons between model and observation. The diagnostic power of satellite simulators has been demonstrated in Kay et al. (2012) and English et al. (2014) by evaluating the Community Atmosphere Model version 5 (CAM5) against a suite of various satellite products. They showed that model cloud biases can be better identified using simulators by excluding the ambiguities in cloud definitions between model and observation. Y. Zhang et al. (2019) also systematically evaluated clouds simulated from the atmosphere component of the DOE Energy Exascale Earth System Model (E3SM, Golaz et al., 2019) version 1 (EAMv1, Rasch et al., 2019; Xie et al., 2018). They found that although EAMv1 performs better than most of the CFMIP models, biases such as the underestimation of optically thin to intermediate clouds and the overestimation of optically intermediate to thick clouds can result in substantial errors in the simulation of cloud radiative effects.

As illustrated in earlier studies (e.g., Y. Zhang et al., 2019; Zhang et al., 2020), EAMv1 largely increases supercooled liquid clouds compared to its predecessor CAM5, leading to overestimated liquid clouds over high-latitude regions in -20°C to -40°C temperature range for both hemispheres. On the other hand, ice cloud fraction is moderately underestimated at temperatures warmer than -40°C. Supercooled liquid fraction (SLF) is therefore substantially larger than CAM5 for temperatures colder than -13°C. The Classical Nucleation Theory (CNT) scheme (Hoose et al., 2010; Wang et al., 2014) used for heterogeneous ice nucleation and the overly reduced Wegner-Bergeron-Findeisen (WBF) process rate were primarily responsible for different cloud phase simulations between EAMv1 and CAM5. With considerable changes in model physics parameterizations and model tuning during the development of E3SM version 2 (E3SMv2) (Golaz et al., 2022) atmosphere model (EAMv2) from its precedent version EAMv1, we would like to examine whether these biases in the simulated cloud phase in EAMv1 are reduced in EAMv2. Enabled by the CALIPSO simulator included in the COSP package in E3SM, we will systematically evaluate model simulated cloud phase against GCM-Oriented CALIPSO Cloud Product (CALIPSO-GOCCP) over both the Arctic and Antarctic regions where mixed-phase clouds prevail. Detailed sensitivity experiments are also designed to understand the physical reasons behind changes in mixed-phase cloud simulation from EAMv1 to EAMv2.

The paper is organized as follows. Section 2 introduces EAMv1 and EAMv2 and the major difference between these two models. The setup of model experiments is also included.

CALIPSO-GOCCP product is described in section 3. Section 4 presents the evaluation of modeled cloud phase in the Arctic and Antarctic, and results of sensitivity experiments are discussed in section 5. Finally, the summary and discussion are provided in section 6.

2. Models and Model Experiments

2.1. EAMv1 Model

EAMv1 serves as the baseline for understanding the EAMv2 model performance. EAMv1 is the atmosphere model of the first version of the U.S. DOE Energy Exascale Earth System Model (Rasch et al., 2019; Xie et al., 2018). EAMv1 runs on the spectral element (SE) dynamical core with 1° horizontal resolution and 72 vertical layers with a top at ~0.1 hPa (64 km). The second version of Morrison and Gettelman (MG2) two-moment bulk microphysics parameterization prognoses mass mixing ratios and number concentrations of cloud hydrometeors (liquid droplet, ice particle, raindrop, and snow particle) and treats complicated microphysical processes in stratiform clouds (Gettelman & Morrison, 2014; Gettelman et al., 2015). The CNT scheme is coupled with MG2 to treat the heterogeneous ice nucleation in mixed-phase clouds (Hoose et al., 2010; Wang et al., 2014). Immersion, deposition, and contact freezing are considered in the CNT scheme, and their freezing rates are determined based on the properties of mineral dust and black carbon aerosols. A probability distribution function (PDF) is considered for the contact angle between dust aerosols and droplets to represent the heterogeneity in immersion freezing ability for individual dust particles. The higher-order turbulence closure scheme CLUBB (Cloud Layers Unified By Binormals) is utilized to unify the treatment of planetary boundary layer turbulence, shallow convection, and cloud macrophysics (Golaz et al., 2002; Larson, 2017; Larson & Golaz, 2005; Bogenshutz et al., 2013). Aerosol properties and aerosol processes are determined by the four-mode version of Modal Aerosol Module (MAM4) (Liu et al., 2012, 2016; Wang et al., 2020). The deep convection scheme follows Zhang and McFarlane (1995) (ZM, hereafter). Other major parameterizations in EAMv1 include a linearized ozone photochemistry mechanism (Linoz2) (Hsu & Prather, 2009) and the Rapid Radiative Transfer Model for GCMs (RRTMG) for the radiative transfer calculation (Iacono et al., 2008; Mlawer et al., 1997).

2.2. Updated Parameterization in EAMv2

Compared to EAMv1, EAMv2 includes several essential upgrades in the model structure and physics parameterizations to improve the model capability of predicting the water cycle and future climate (Golaz et al., 2022). One major change is the use of separate parameterized physics and dynamics grids (Hannah et al., 2021). The average horizontal grid spacing is ~110 km for the dynamic grid and ~165 km for the physics grid. This new physics grid has little impact on modeled climate, but it is one of the two main factors (the other is a new semi-Lagrangian passive tracer transport) that makes EAMv2 approximately two times faster than EAMv1.

Several important changes are made for the model physics. The second version of CLUBB (CLUBBv2) is implemented in EAMv2 (Larson, 2017). CLUBBv2 shares the same philosophy as CLUBBv1, but it includes new options to enhance CLUBB's gustiness and prognostic treatment of momentum fluxes. The call of estimates of CLUBB's PDF is also moved to a position ahead of advancing CLUBB's predictive fields, so that saturation is adjusted before the calculation of microphysics. For deep convective clouds, a new convection trigger function is incorporated in the ZM scheme in EAMv2 (Xie et al., 2019; Wang et al., 2020). The new trigger emphasizes the controlling role of the dynamic Convective Available Potential Energy (dCAPE) (Xie & Zhang, 2000) due to large-scale advective tendencies of temperature and moisture on the convective onset, and also includes the Unrestricted Launch Level (ULL) feature allowing the initiation for both surface-driven convection and elevated convection between surface and 600 hPa (Wang et al., 2015). Following Ma et al. (2021), a number of tuning parameters are recalibrated in CLUBB, ZM deep convection, and microphysics schemes to improve the simulation of cloud and precipitation. To improve the representation of surface exchanges of heat, moisture, and momentum over land and ocean, subgrid-scale treatment for surface wind gustiness is also incorporated following the formulation from Redelsperger et al. (2000) (Harrop et al., 2018; Ma et al., 2021). Meanwhile, the emitted size distribution of mineral dust is modified to allow more emissions of coarse dust to the atmosphere (Feng et al., 2022); and the dust refractive indices in the shortwave bands are updated using derived values from the AERONET measurements (Dubovik et al., 2000). A new ozone (O_3) module is introduced to preserve the sharp cross-tropopause gradient and improve the stratosphere-troposphere exchange flux of O_3 (Tang et al., 2021). Other changes in model physics include implementing a minimum cloud droplet number concentration (CDNC) of 10 cm^{-3} in cloud microphysics and retuning the gravity wave drag parameters. See Golaz et al. (2022) for details about the EAMv2 model.

2.3. Model Experiments

In this study, 11 years of free-run simulations are performed using EAMv1 and EAMv2 with prescribed CMIP6 anthropogenic emissions and present-day climatologies of sea ice and sea surface temperature. The last 10-year simulations are used in the model analyses. Sensitivity experiments are designed to isolate the impact of new changes in EAMv2 on simulated mixed-phase clouds. Table 1 lists the default EAMv1 and EAMv2 experiments as well as sensitivity experiments for the four selected changes made in EAMv2. A complete list of parameters that changed from EAMv1 to EAMv2 is provided in the supplementary material (Table S1) and can also be found in the Appendix of Golaz et al. (2022).

The sensitivity experiments are based on EAMv2, and the four newly introduced model features are individually reverted to their EAMv1 settings to examine their effects on cloud phase simulation. The four changes include 1) the scaling factor on the WBF process, 2) the new trigger function for deep convection initiation, 3) the tuning parameters associated with deep convection, and 4) the minimum CDNC. First. as discussed in M. Zhang et al. (2019), modifying the WBF process can significantly alter the phase partitioning of mixed-phase clouds in CAM5. Y. Zhang et al. (2019) found that the scaling factor on the WBF process was unreasonably set to 0.1 to slow down the WBF process, which led to a considerable underestimation of ice clouds in EAMv1. To address this issue, the parameter is recalibrated to 0.7 in EAMv2, which is carried over from Ma et al. (2021). In the experiment “WBF01”, we revert the parameter back to 0.1 to examine its impact on the simulation of cloud phase. Second, the detrained cloud water from deep convection can substantially influence stratiform cloud microphysics as the detrained cloud water to stratiform clouds can initiate the following cloud microphysical processes (Zhang et al., 2013; Zhang & Bretherton, 2008). Using the new dCAPE_ULL convective trigger in EAMv2 can thus impact model convective activities and then stratiform cloud microphysical processes through detained cloud water from deep convection over the polar regions (Zhang et al., 2005). In this study, we conduct the experiment “CAPE_Trigger” by replacing the new dCAPE_ULL trigger with the original CAPE trigger in EAMv2 to study its impact. Third, as noted in Ma et al., (2021) and Golaz et al., (2022), several tuning parameters are recalibrated for ZM deep convection scheme. To test the effect of these parameters on high latitude clouds, the experiment "ZM_Tuning" is performed by setting these parameters to values that are used in EAMv1. Finally, EAMv2 implemented a minimum CDNC in cloud microphysics. Microphysical processes related to cloud liquid water can be largely affected due to the change in CDNC. The experiment "No_Mincdnc" is conducted by removing the minimum threshold (10 cm^{-3}) to understand the impact of this change. Other changes made in EAMv2 are also tested, but they have relatively minor impacts on the simulated cloud phase at high latitudes.

Table 1. List of model experiments and parameter settings in EAMv2 and EAMv1

Model Experiment	Model Setup
EAMv2	Default EAMv2 model
EAMv1	Default EAMv1 model
WBF01	Same as EAMv2, but set the scaling factor on WBF process from 0.7 to 0.1
CAPE_Trigger	Same as EAMv2, but turn off the new dCAPE_ULL trigger and use the EAMv1 CAPE trigger
ZM_Tuning	Same as EAMv2, but set tuning parameters related with deep convection to values used in EAMv1
No_Mincdnc	Same as EAMv2, but reset the minimal number for cloud droplet (CDNC) from 10 cm^{-3} to 0

3. CALIPSO-GOCCP Data

We use the 2006-2012 CALIPSO-GOCCP climatology dataset (version 2.68) (Chepfer et al., 2010) in the model evaluation. The CALIPSO-GOCCP product was developed particularly for evaluating clouds from the CALIPSO simulator, which is part of the COSP satellite simulator package (Chepfer et al., 2008). It uses the measured total attenuated backscattered signal (ATB) profiles at 532 nm from the Level 1 data of the Cloud-Aerosol Lidar with Orthogonal Polarization (CALIOP), onboard the CALIPSO satellite (Winker et al., 2007, 2009). The atmospheric profiles from the Goddard Modeling and Assimilation Office (GMAO) are used to derive the molecular ATB profiles in the atmosphere free of clouds and aerosols (Bey et al., 2001). Both ATB and molecular ATB profiles are averaged onto 40 vertical grids with height intervals at 480 m and have a horizontal resolution of 330 m. Following the same algorithm in the CALIPSO simulator, lidar scattering ratio (SR) profiles are derived by dividing the ATB profile by the molecular ATB profile for cloud detection. Each vertical layer is labeled using different SR thresholds as cloudy ($SR > 5$), clear ($0.01 < SR < 1.2$), unclassified ($1.2 < SR < 5$), and fully attenuated ($SR < 0.01$). In addition, cloud phase is identified with an empirical phase discrimination function between cross-polarized ATB ($ATB_{\perp}$) and ATB measured from the CALIOP lidar. The phase discrimination is physically based on the difference in the change of state of polarization of laser signal that backscattered after encountering liquid and ice particles (Cesana & Chepfer, 2013). To facilitate the direct comparison with GCM outputs, monthly cloud fraction data is diagnosed over a typical GCM grid box of 2° × 2° horizontal resolution. The monthly statistics of grid-mean total cloud fraction and cloud fraction in the diagnosed phase (i.e., liquid, ice, and undefined) are summarized over a GCM grid box by dividing the number of cloudy subcolumns during one month by the number of subcolumns that are not fully attenuated during the same month. More details about the CALIPSO-GOCCP retrievals can be found in Chepfer et al. (2010) and Cesana and Chepfer (2013).

4. Evaluation of Clouds

4.1. Global Cloud Cover

Figure 1 shows the CALIPSO-GOCCP annual mean total cloud cover and cloud cover biases in EAMv2 and EAMv1 simulations diagnosed from the CALIPSO simulator. Consistent with earlier studies (Rasch et al., 2019, Xie et al., 2018, Y. Zhang et al., 2019), EAMv1 largely underpredicts total cloud cover over the tropical and extratropical regions. Cloud cover is much lower than CALIPSO-GOCCP over the west coasts of major continents in the subtropical regions where marine stratocumulus clouds are prevalent. Negative biases are also found over the tropical western Pacific area and over tropical and mid-latitude lands. With updated physics parameterizations and model tuning parameters, EAMv2 shows considerable improvements in simulating marine stratocumulus clouds near the west coasts of continents. Negative cloud bias over subtropical lands and positive bias over the SO are also improved in EAMv2. However, simulated clouds over the tropical Indian Ocean and subtropical Pacific Ocean become degraded. In the Arctic, the excessive clouds produced by EAMv1 remain in EAMv2. In the following sections, we will focus on high-latitude regions where mixed-phase clouds are present in most of the year and have not been extensively evaluated in Golaz et al. (2022). We aim to understand how the simulated cloud phase in EAMv2 differs from EAMv1 and the reasons behind the identified differences. The improved understanding of the model behavior change from EAMv1 to EAMv2 will provide valuable information for future E3SM developments.

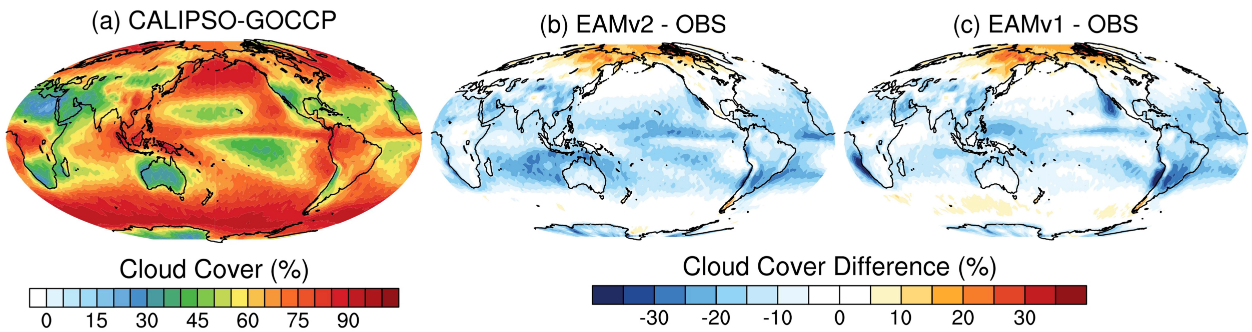

Figure 1. Global map of annual mean total cloud cover from (a) CALIPSO-GOCCP and the total cloud cover difference between observation and CALIPSO simulator from (b) EAMv2 and (c) EAMv1.

4.2. Arctic Cloud Cover and Cloud Phase

Figure 2 shows the North Pole map (poleward of 60°N) of annual mean total cloud cover and cloud cover in liquid and ice phases. Consistent with early observations (Shupe et al., 2006; Zhang et al., 2018), CALIPSO-GOCCP shows ubiquitous cloud coverage in the Arctic. There is a strong land-ocean contrast in the spatial distribution of cloud phase. For example, a larger liquid cloud fraction is observed over the ocean, while ice phase clouds are more extensive over lands. The maximum liquid-containing clouds can have up to 60% coverage near the Norwegian Sea and Barents Sea, dominating the observed total cloud cover in these regions. On the other hand, large ice cloud cover (up to 40%) is found over Greenland, North America, and Siberia.

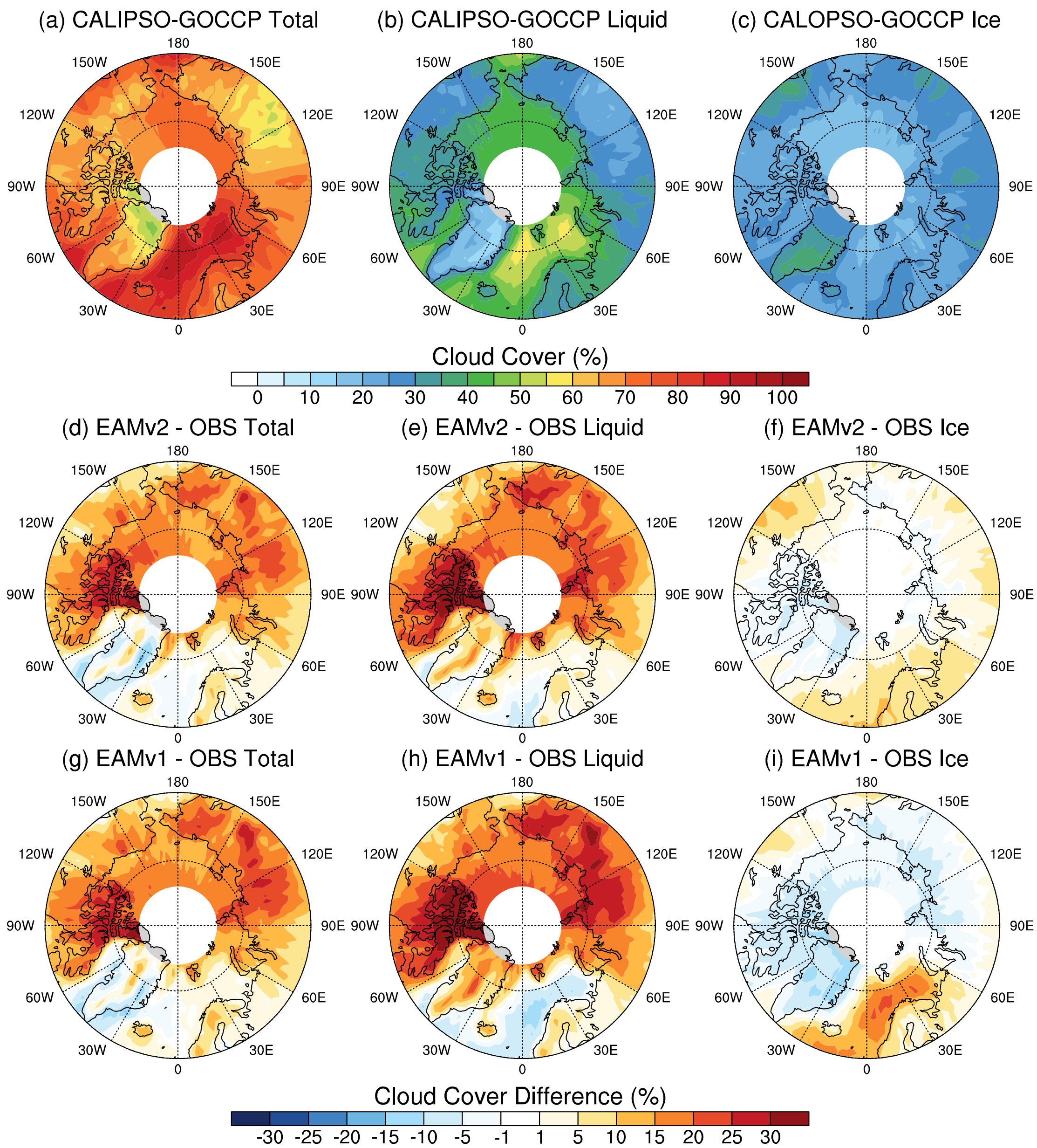

Figure 2. Arctic polar map of annual mean observed cloud cover in (a) total, (b) liquid phase, (c) ice phase from CALIPSO-GOCCP. Differences between CALIPSO simulator generated total cloud cover and CALIPOS-GOCCP are shown in (d) for EAMv2 and (g) for EAMv1. Differences in the liquid phase and ice phase are shown in (e) and (f) for EAMv2 and (h) and (i) for EAMv1, respectively.

The CALIPSO-GOCCP observed contrast in cloud phase between ocean and land in the Arctic is overall captured by EAMv2 and EAMv1 (figure not shown). However, total cloud cover and cloud phase predicted by both models are substantially biased. As shown in Section 4.1, both EAMv2 and EAMv1 overestimate total cloud cover over nearly the entire Arctic except Greenland, Norwegian Sea, and Barents Sea. In both models, these large positive biases are mainly contributed from the overestimation of liquid clouds. Due to the decreased positive liquid cloud bias, the overly predicted total clouds in EAMv2 are slightly smaller than those in EAMv1. For ice clouds, cloud ice is moderately underestimated in EAMv1 over most of the Arctic. Such a bias has been mostly reduced in EAMv2. As shown in Figure 2f, minimal bias is found over the Arctic Ocean and Greenland compared to CALIPSO-GOCCP, although ice clouds become somewhat overestimated over major Arctic lands. Another significant improvement in the simulated cloud phase exists over the Norwegian Sea and Barents Sea. It is clear that ice (liquid) cloud cover is too large (few) in EAMv1, and these biases are largely reduced in EAMv2.

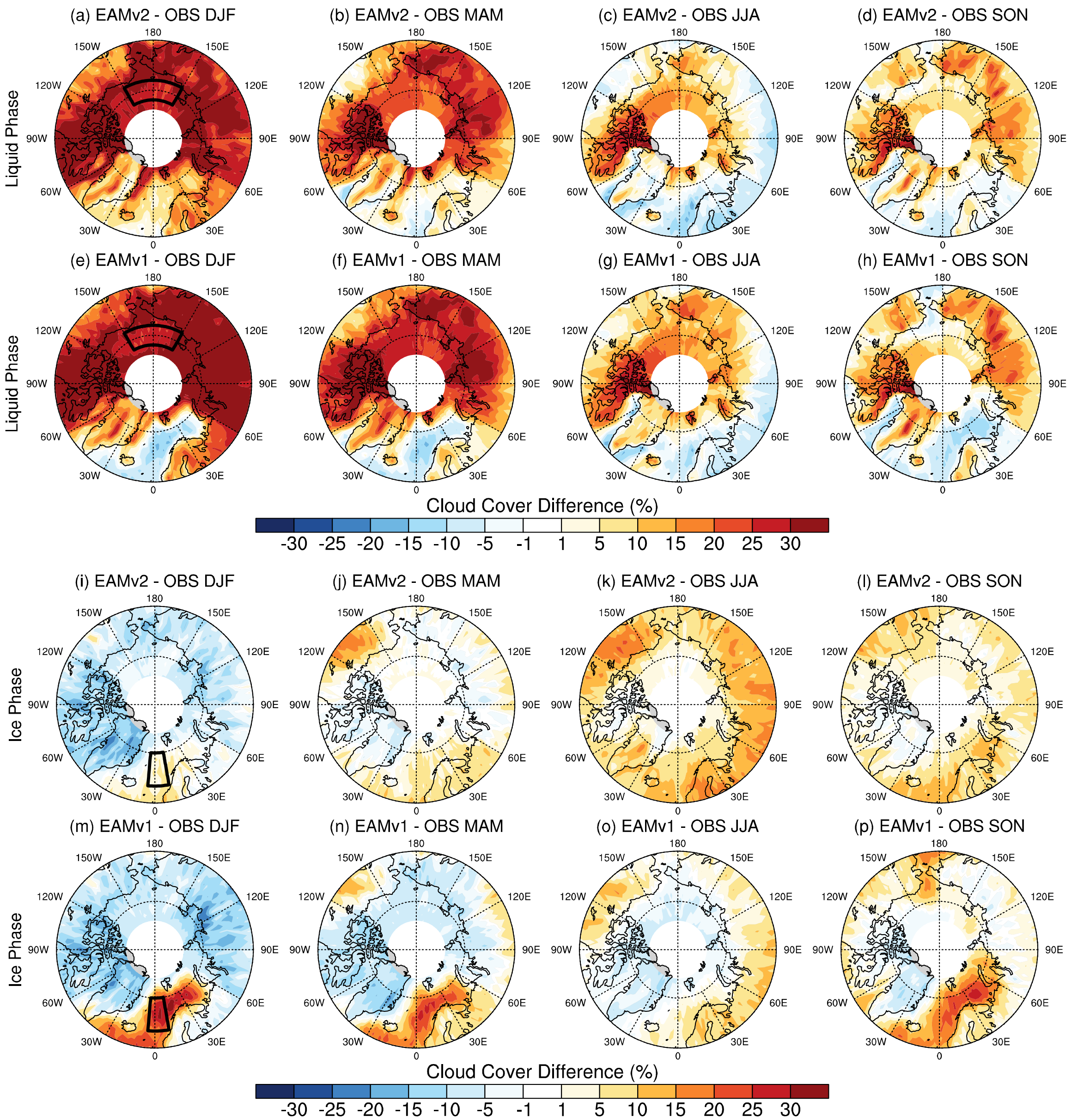

Figure 3. Arctic polar map of seasonal cloud cover biases between CALIPSO-GOCCP and EAMv2 and EAMv1. (a)-(d) and (e)-(h) are for EAMv2 and EAMv1 liquid clouds, respectively, while (i)-(l) and (m)-(p) are for ice clouds. Cloud cover and cloud phase from EAM models are predicted using the CALIPSO simulator. Black boxes shown in (a) and (e) represents the location of vertical profiles analyzed in Figure 4, while black boxes in (i) and (m) are shown for the location analyzed in Figure 5.

The simulated cloud phase bias shows strong seasonal variations (Figure 3). Although the overestimation of liquid clouds is common across the year, both models show the most prominent biases in boreal winter and spring (i.e., DJF and MAM). These positive biases in liquid clouds are moderately reduced in EAMv2. During the same seasons (DJF and MAM), the modeled ice clouds are considerably under-predicted over most of the Arctic region in EAMv1. EAMv2 also to some extent reduces these negative biases. However, the ice clouds produced by EAMv2 are larger than the observations in summer and fall (i.e., JJA and SON). Over the Norwegian Sea and Barents Sea, it is interesting to note that cloud phase biases in EAMv1 differ significantly from the rest of the Arctic during winter, spring, and fall. For instance, the overestimation of ice clouds and underestimation of liquid clouds are found in all three seasons in EAMv1, which is opposite to the other regions. Compared to EAMv1, EAMv2 substantially alleviates these biases in cloud phase by decreasing (increasing) simulated ice (liquid) clouds over the Norwegian Sea and Barents Sea. We note that Arctic liquid cloud cover has a strong seasonal variation in CALIPSO-GOCCP, with the highest (lowest) cloud amounts in summer (winter). However, the contrast in simulated cloud cover between winter and summer is less significant in both models (Figure S1). With more constant cloud covers simulated throughout the years, a larger positive bias of liquid cloud cover is thus produced during boreal winter and spring in EAMs.

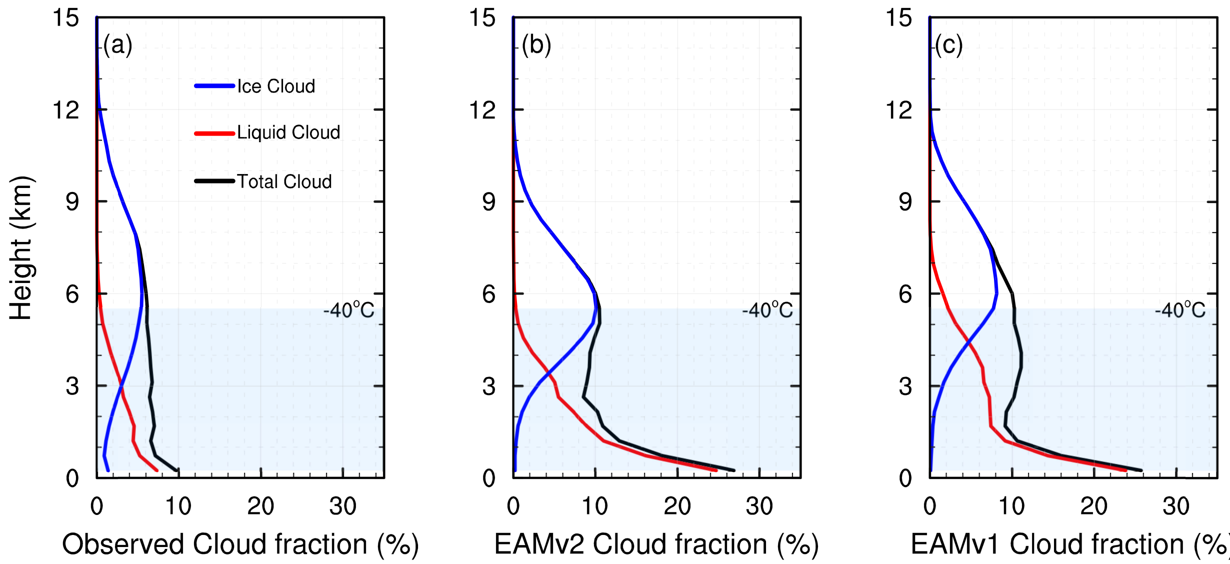

Figure 4. Vertical profiles of total cloud cover (black), liquid cloud cover (red), and ice cloud cover (blue) over the Arctic Ocean. Cloud profiles are averaged in boreal winter (i.e., DJF) over the locations shown in black boxes in Figures 3(a) and 3(e). Profiles in (a)-(c) are for CALIPSO-GOCCP, EAMv2, and EAMv1, respectively. Blue shaded area represents the mixed-phase cloud temperature range (0 — -40°C) in ERA5 reanalysis data and EAM models.

To better understand these model errors in the simulated cloud phase, cloud profiles are generated to quantify the bias in vertical structures. We first present the vertical structure of averaged clouds over the Arctic Ocean during the boreal winter (i.e., DJF) when the maximum bias in liquid cloud cover occurs in the EAM simulations. The location of averaged profiles is shown in Figures 3a and 3e, which represents the Arctic maritime condition. We also examined the cloud profiles under the Siberia and North America continental conditions. Because these three locations reveal similar results, only the cloud profiles under the maritime condition are presented here. As shown in Figure 4, clouds are observed at layers up to 12 km. Supercooled liquid clouds are predominantly found at lower altitudes (< 5 km), with increased liquid cloud fraction approaching the surface. Ice clouds dominate at mid to high altitudes (> 3 km), and these clouds are in the mixed-phase regime below ~5.5 km. The two EAM models predict the correct locations of supercooled liquid clouds, in good agreement with CALIPSO-GOCCP. However, the simulated liquid cloud fractions are larger than observations particularly at layers below 1 km. Positive bias in these low-level liquid clouds largely contributes to the bias in total cloud cover. The strong correlation between biases in low-level liquid clouds and total clouds (figure not shown) confirms that the excessive low-level supercooled liquid clouds is the primary reason for the overestimation of clouds over the Arctic Ocean, North America, and Siberia regions.

Cloud vertical profiles in Figure 4 also provide insights into the cause of underestimation of ice clouds in both EAMs over the Arctic Ocean. It is shown that both models have insufficient ice clouds at lower altitudes (< 2 km) compared to CALIPO-GOCCP. Although there are too much ice clouds at altitudes between 4 and 8 km in both models, the underestimated ice clouds in the lower troposphere likely lead to the negative bias shown in Figure 3. Meanwhile, Figure 4 shows that ice cloud fraction between 4 and 6 km is increased in EAMv2. Such an increase in ice clouds is responsible for the overall reduction of negative ice cloud bias shown in Figure 3.

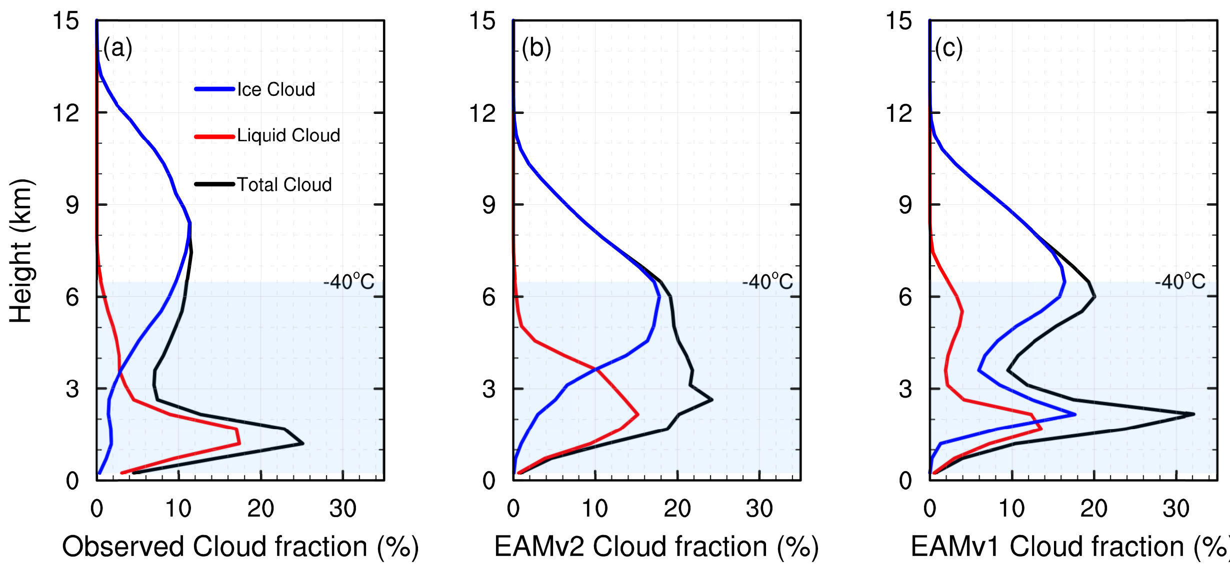

Figure 5. Same as Figure 4 but for cloud profiles averaged over the Norwegian Sea during boreal winter. The location of the profile is shown in Figures 3(i) and 3(m).

To understand the change in simulated cloud phase between EAMv1 and EAMv2 over the Norwegian Sea and Barents Sea, we examine the vertical profiles of cloud cover averaged over the region indicated by black boxes in Figures 3i and 3m. The Arctic winter (i.e., DJF) is again selected due to the maximum cloud bias. Even though the observed feature that ice (liquid) clouds peak at higher (lower) altitudes is captured in both models, EAMv1 shows a second peak of ice cloud at ~2 km in Figure 5c, which is not evident in CALIPSO-GOCCP and EAMv2. The presence of the spurious "dual peak" vertical structure in EAMv1 contributes to the overestimation of ice clouds shown in Figures 2 and 3. As revealed in the sensitivity experiments (Section 5), the newly introduced dCAPE_ULL trigger in the ZM scheme is the primary reason for removing the unrealistic ice cloud layer in EAMv2. Furthermore, although the second peak in the ice cloud structure is eliminated, the ice clouds in EAMv2 are still biased. Figure 5 shows that the height where ice (liquid) cloud cover peaks is too low (high) in EAMv2 compared to CALIPSO-GOCCP. The ice cloud cover is also overestimated in the mixed-phase cloud temperature range (i.e., 0 – -40°C), whereas it is underestimated in the cirrus temperature range (< -40°C). The compensating errors from different cloud types require further analysis.

4.3. Clouds over SO and Antarctic

The SO and Antarctic are the other regions where mixed-phase clouds prevail. Figure 6 shows the South Pole map (poleward of 60°S) of annual mean cloud cover observed by CALIPSO-GOCCP and the biases in CALIPSO simulator-derived clouds from EAMv2 and EAMv1. CALIPSO observations show that clouds are extensive (cloud cover > 90%) over the SO, while there are relatively fewer clouds (cloud fraction < 60%) over Antarctica. Like the Arctic, liquid-containing clouds are pronounced over the ocean with an annual mean coverage of up to 50%. On the other hand, ice clouds are commonly found (cloud fraction ~40%) over the Antarctic land.

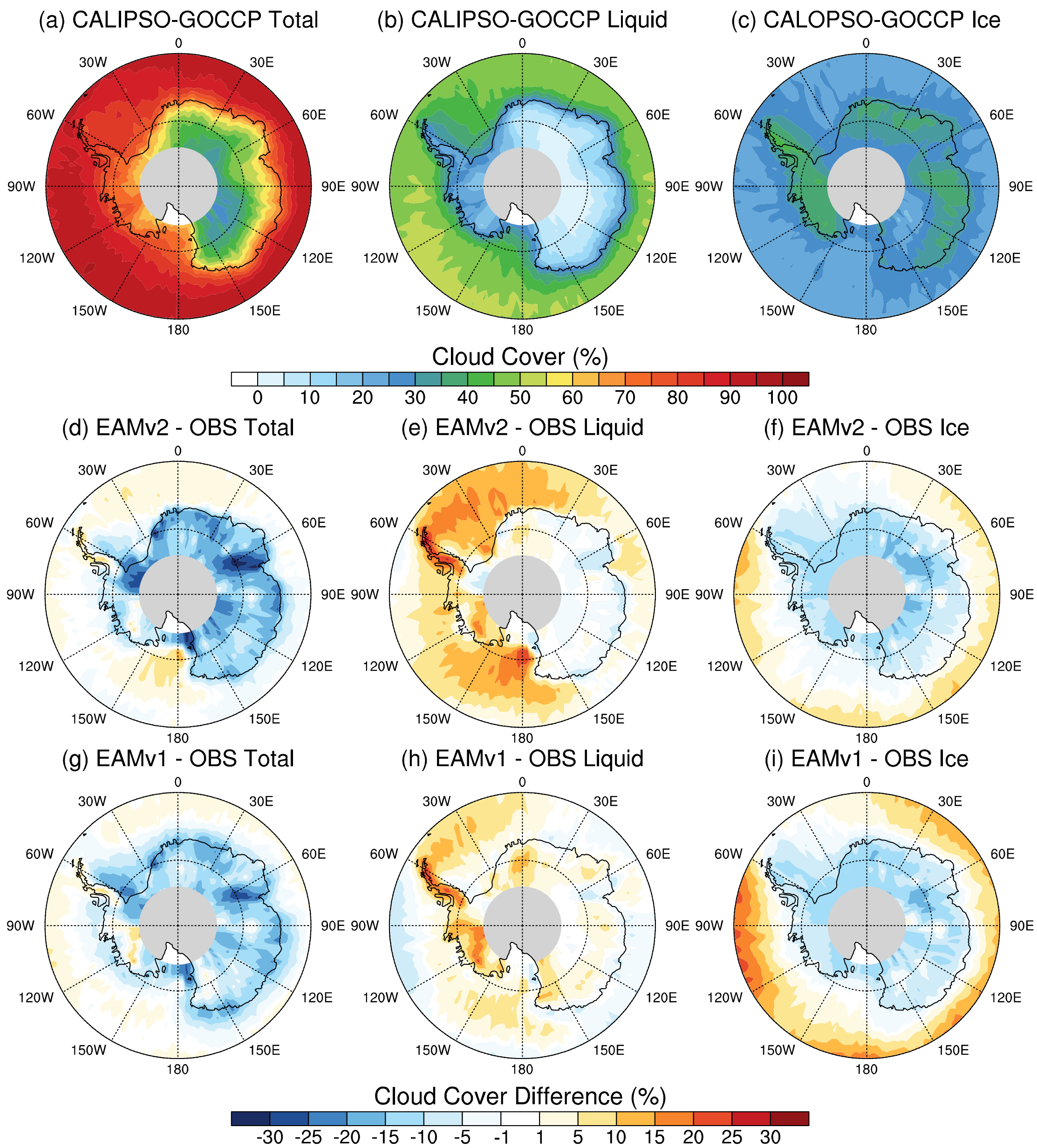

Figure 6. Same as Figure 2 but for the observed cloud cover and cloud cover biases between model and observation in the Antarctic polar map.

Compared to CALIPSO-GOCCP, EAMv2 and EAMv1 behave similarly regarding the annual mean total cloud cover, with small positive biases over the SO and large negative biases over the Antarctic land. Over the SO, the bias in liquid clouds generally shows an opposite sign to that in ice clouds in both models, indicating error compensations in total cloud covers. However, over the Antarctic land, the underestimation of total cloud cover is mainly due to the under-predicted ice clouds in both models. It is seen that EAMv2 improves the simulation of ice clouds, especially over the SO, while it shows larger positive bias in liquid clouds over the SO.

Differences in the simulated cloud phase between EAMv2 and EAMv1 are more evident in their seasonality. Figure 7 indicates that the positive bias of liquid clouds from EAMv2 is substantial in all seasons. The feature that liquid cloud bias is larger in colder seasons (i.e., JJA and SON) is consistent with what has been discussed for the Arctic. Also consistent with the Arctic, the overestimation of supercooled liquid clouds near the surface mainly contributes to the positive bias in both liquid clouds and total clouds in EAMv2 over the SO (figure not shown). Conversely, insufficient liquid clouds in EAMv1 over the SO during austral summer and fall (i.e., DJF and MAM) offsets the overestimation of liquid clouds during austral winter and spring (i.e., JJA and SON), making the annual liquid clouds generally comparable to observations except over the Weddell Sea, the Amundsen Sea, and the Ross Sea. This underestimation of liquid clouds in EAMv1 closely corresponds to the overestimation of ice clouds in the lower troposphere (2−3 km) over the SO off the Antarctic continent (figure not shown). Intrigued by the comparable ice cloud biases over the Norwegian and Barents Sea in the Arctic, the suppression of deep convection initiation with the new trigger is found to substantially modify cloud microphysical processes for cloud liquid and ice. This mechanism significantly changes the cloud phase simulation over the open oceans in both hemispheres. A process-level analysis will be discussed in Section 5.

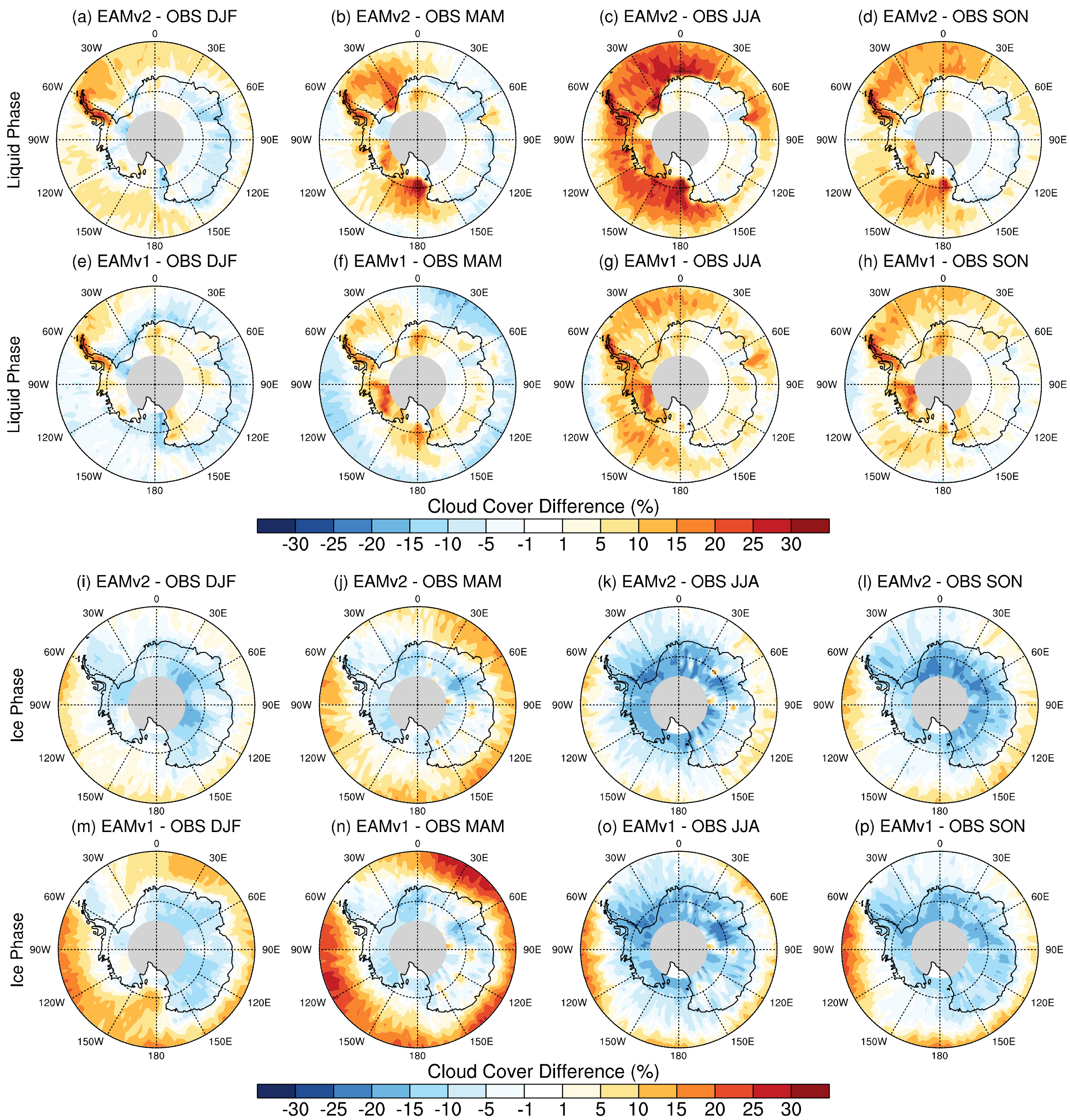

Figure 7. Same as Figure 3 but for the Antarctic cloud cover biases in the liquid phase and ice phase.

Over the Antarctic land, although liquid-containing clouds are less dominant than ice clouds, EAMv2 reasonably predicts liquid cloud covers in all seasons, which is slightly improved compared to EAMv1 (Figure 7). Substantial low biases are found in ice clouds all year round in both models. The underestimation of ice clouds dominates total cloud errors as shown earlier. The cross-section analysis indicates that both models predict insufficient high-level (> 10 km) ice clouds over Antarctica (figure not shown), which is likely the reason for the underestimation of ice clouds presented on the Antarctic land.

5. Model Sensitivity Experiments

To further understand the reasons for the improved cloud phase in EAMv2, a set of sensitivity experiments (Table 1) are performed based on the EAMv2 model. The design of each sensitivity experiment has been introduced in Section 2.3.

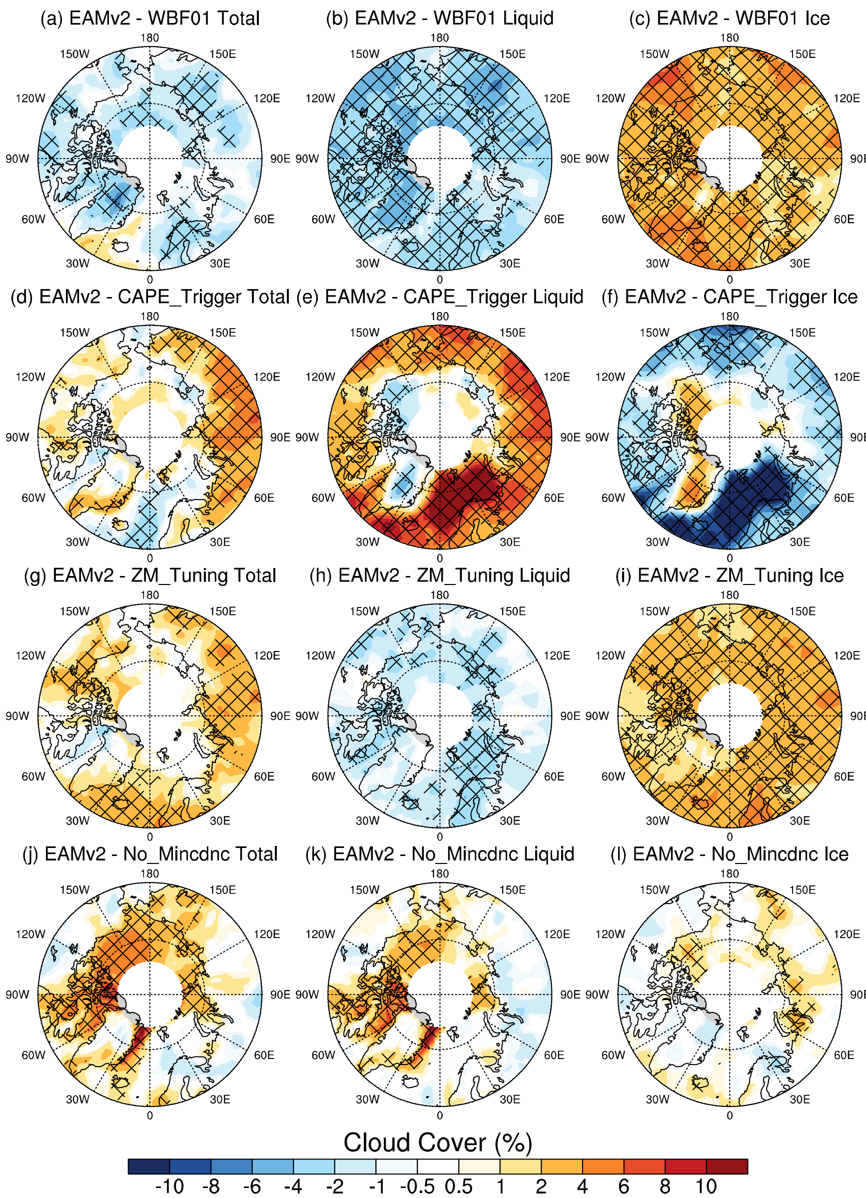

Figure 8. Arctic polar map of annual cloud cover difference between sensitivity experiments and the default EAMv2 experiment. The left column is for total cloud cover, the middle column is for liquid cloud cover, and the right column is for ice cloud cover. (a)-(c) shows the experiment using the scaling factor of 0.1 on the WBF process; (d)-(f) shows the experiment without the new dCAPE_ULL trigger; (g)-(i) shows the experiment that sets the tuning parameters in deep convection to values that are used in EAMv1; and (j)-(l) removes the minimum CDNC in cloud

microphysics. Black crosses indicate regions that are statistically significant at the 90% confidence level.

For clouds in the Arctic, sensitivity experiments (Figure 8) indicate that changing the scaling factor of the WBF process from 0.1 (default in EAMv1) to 0.7 (default in EAMv2) significantly decreases liquid and increases ice cloud over the entire Arctic. Total cloud cover is also decreased due to the enhanced glaciation of mixed-phase clouds. This is expected because an increased WBF process rate can result in more occurrence of the total consumption of liquid water in mixed-phase clouds and thus decrease cloud lifetime (M. Zhang et al., 2019). Conversely, while recalibrated parameters for ZM scheme also increase ice cloud and decrease liquid cloud, simulated total cloud cover is increased as shown in Figure 8g. Reduced convective autoconversion efficiency and decreased ice particle size detrained from deep convection probably prolong the lifetime of ice clouds (Ma et al., 2021). Note that the decrease of liquid cloud due to the modified WBF process scaling factor and ZM tuning is largely canceled out by the introductions of the new dCAPE_ULL trigger and the minimum CDNC. Figure 8 shows that the new convective trigger plays an essential role over the Arctic lands, Norwegian Sea, and Barents Sea, while the minimum CDNC is more influential over the Arctic Ocean. As discussed in earlier sections, the overestimation of liquid cloud cover is an outstanding issue for both models over the Arctic Ocean. However, even though the No_Mincdnc experiment gives a lower liquid cloud fraction than the default EAMv2 over the Arctic Ocean, supercooled liquid clouds are still overestimated near the surface without changing liquid cloud profiles (Figure 9d). Cloud profiles over the Arctic Ocean are also insensitive to the other three sensitivity experiments (Figures 9a-9c), implying the role of other factors in this bias.

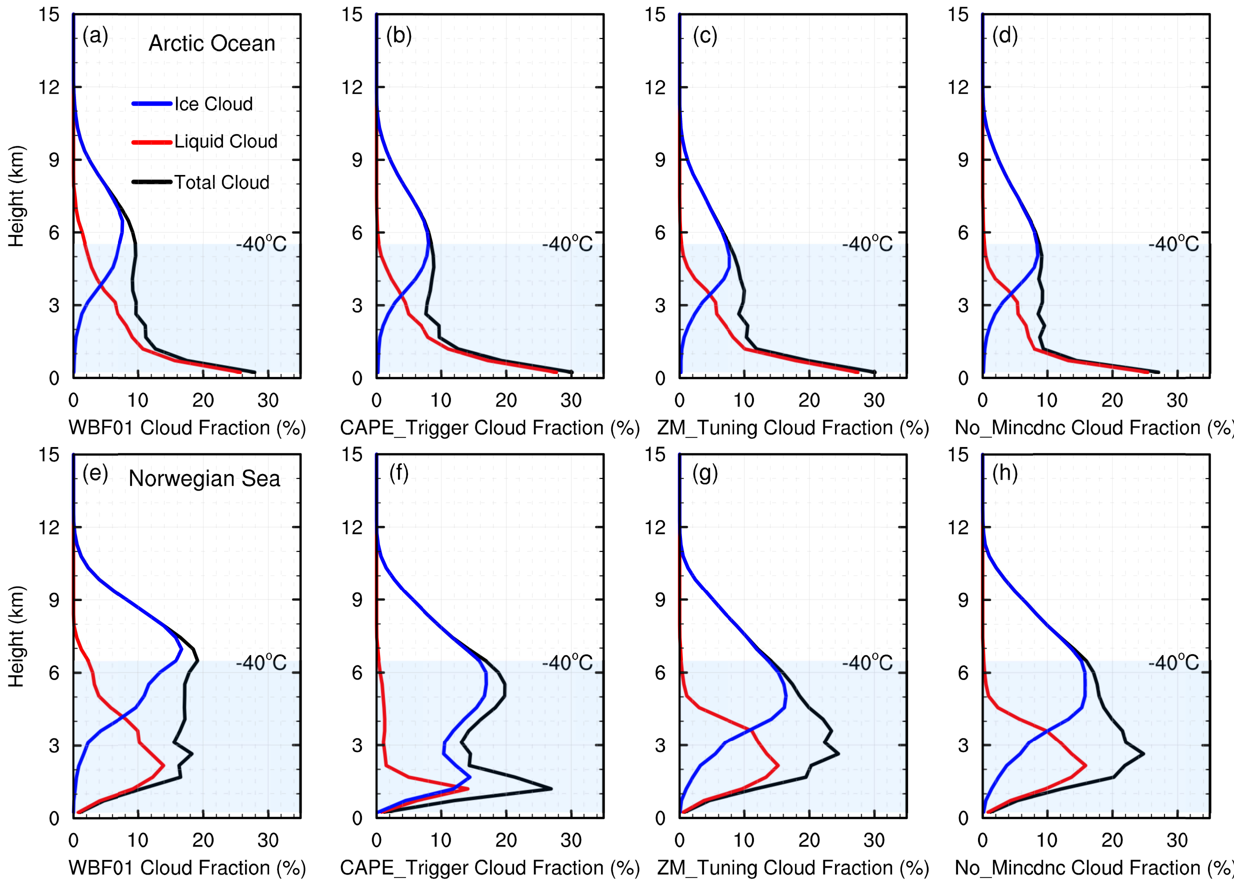

Figure 9. Vertical profiles of averaged cloud cover from sensitivity experiments. (a)-(d) are profiles over the Arctic Ocean with the same location and season shown in Figure 4. (e)-(h) are profiles over the Norwegian Sea; and the location and season are the same as Figure 5.

In terms of the model cloud fraction change over the Norwegian Sea, the new trigger significantly reduces the cloud phase error shown in EAMv1. This is confirmed by the fact that the CAPE_Trigger experiment, which turns off the new trigger, reproduces the spatial distribution of cloud phase biases in EAMv1 and the “dual peaks” in the ice cloud vertical profile (Figure 9f). Further analysis suggests that the impact of the modified ZM scheme on simulated cloud phase mainly results from the reduced deep convection initiation. Xie et al. (2019) demonstrated that by introducing a dynamic constraint on convection initiation, the convection becomes less frequently triggered. As shown in Figure 10, convection contributes more to total precipitation in EAMv1 compared to EAMv2. Especially over the Norwegian and Barents Sea where cloud phase biases are substantial, convective precipitation occurs more frequently in EAMv1 and CAPE_Trigger than EAMv2. Through a separate one-year simulation test with deep convection related fields saved at each model time step, we found the initiation frequency of ZM scheme is reduced by 70-80% over the Norwegian and Barents Sea when the dCAPE_ULL trigger is used. However, how deep convection from ZM is linked to the E3SM cloud phase simulation needs a further analysis.

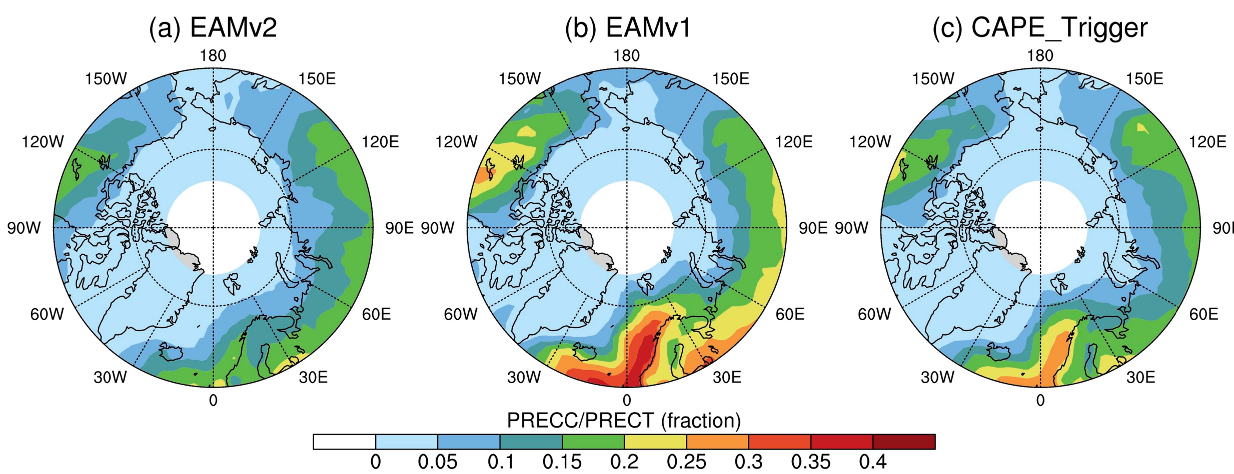

Figure 10. Arctic polar map of the annual fraction of convective precipitation rate over total precipitation rate. Results of EAMv2, EAMv1, and EAMv2 with the new trigger turned off are shown in (a), (b), (c), respectively.

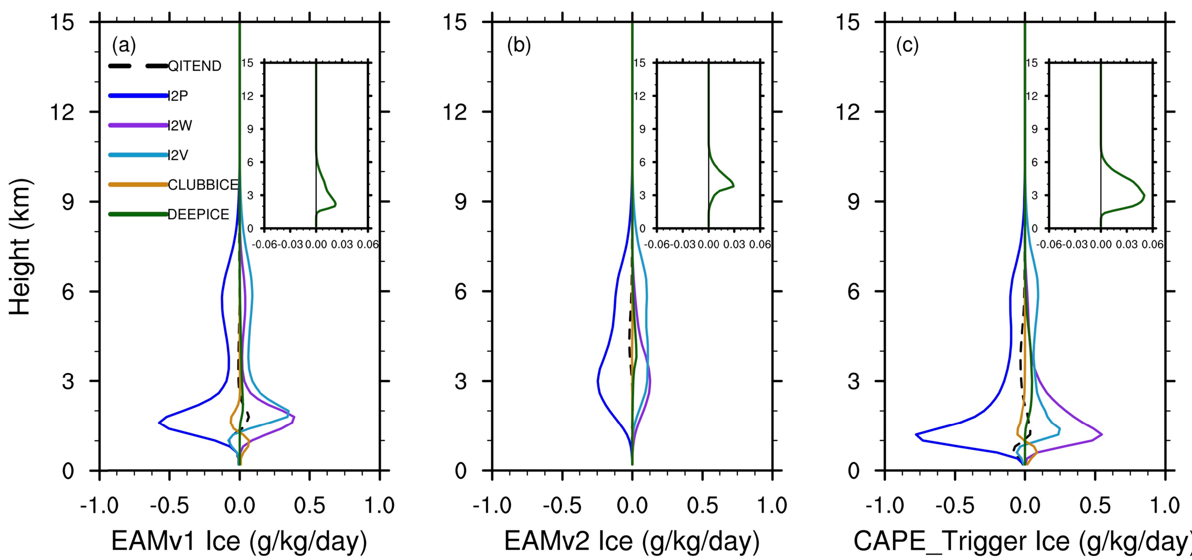

Figure 11. Profiles of ice-related process tendency rates from EAMv1 (left), EAMv2 (middle), and EAMv2 without the new trigger (right). Profiles are averaged over the Norwegian Sea with the same location and time period as Figure 5. Detrained ice from deep convection (DEEPICE, green) is highlighted in the right corner of each panel. The total tendency rate of ice processes (QITEND, dashed black), conversion rates between cloud ice and precipitation (I2P, blue), cloud liquid (I2W, purple), and water vapor (I2V, light blue), and cloud ice calculated in turbulent transport in CLUBB (CLUBBICE, dark orange) are shown.

A simple treatment of cloud microphysics is used in the ZM deep convection parameterization. In both EAMv2 and EAMv1, once convection is triggered, cloud water is detrained from deep convection to stratiform clouds. Detrained water is partitioned as pure liquid when temperature is warmer than 268.15 K, and as pure ice when temperature is colder than 238.15 K with a linear interpolation in between. Figure 11 clearly shows that the peak of ice cloud cover at ~2 km in EAMv1 (shown in Figure 5) corresponds well with the large process rate of detrained ice. Detrained ice from deep convection peaks at a much higher altitude in EAMv2, and the lower altitude peak is reproduced when the new trigger is turned off. With increased cloud ice detrained from deep convection, process rates for the mass conversion from liquid and vapor to cloud ice (i.e., I2W and I2V) are significantly accelerated in EAMv1 and CAPE_Trigger. This further proves our hypothesis that detrained ice water caused by the too frequent trigger of deep convection is the main reason for cloud phase biases over the Norwegian and Barents Sea in EAMv1.

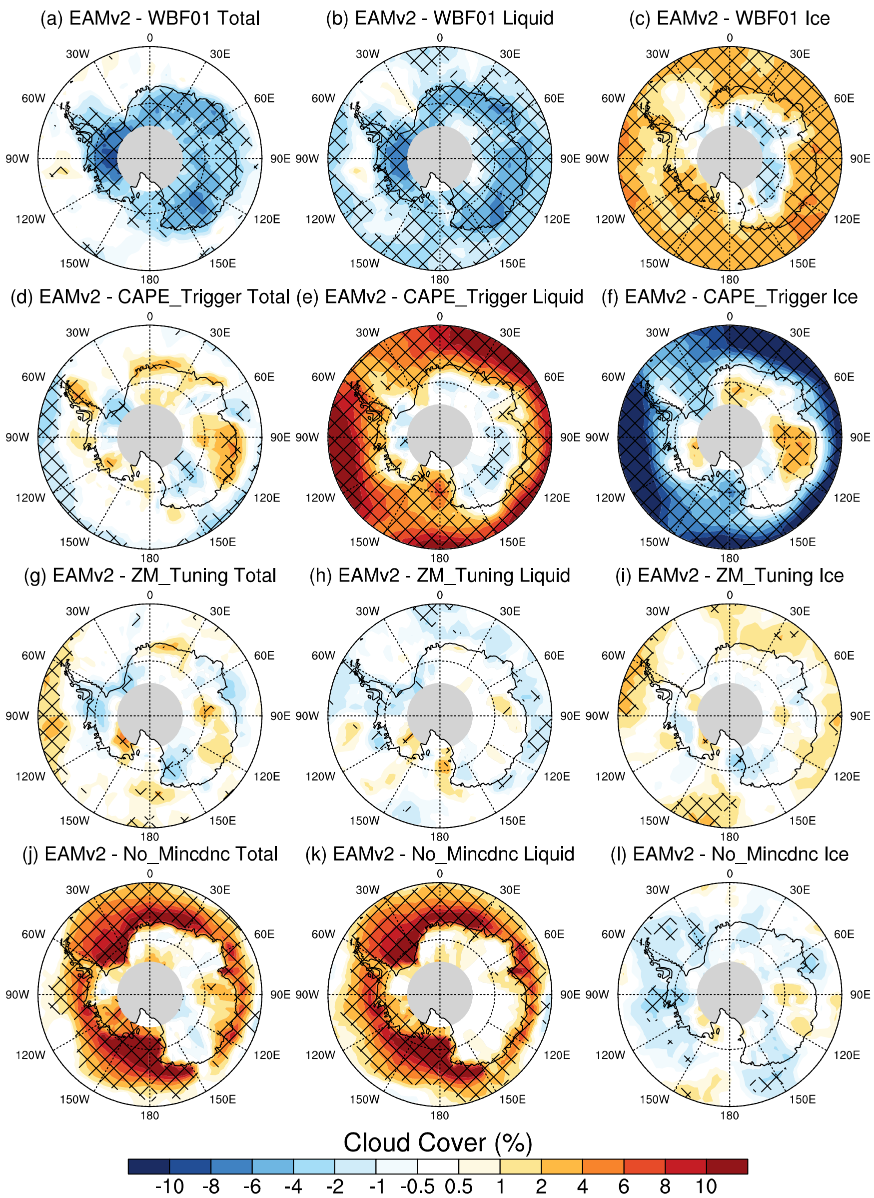

Figure 12. Same as Figure 8 but shows the Antarctic polar map.

For simulated cloud phase changes over the SO and Antarctic region, sensitivity experiments reveal that the effects from the scaling factor of the WBF process, the new dCAPE_ULL trigger, and the minimum CDNC are generally consistent to those in the Arctic

(Figure 12). For example, the WBF scaling factor (0.7) decreases liquid and increases ice clouds nearly over the entire SO, but both the new trigger and the minimum CDNC offset this changed cloud phase. It is clear from Figure 12 that the new trigger plays a similar role over the SO compared to Norwegian and Barents Seas, which substantially reduces the excessive ice clouds identified in EAMv1. However, the modified trigger together with the minimum CDNC also contribute to the too large liquid clouds over the SO. It is interesting that, despite of the noticeable impact from ZM related tuning parameters on cloud phase in the Arctic, these parameters have minimal effects on simulated clouds at high latitudes in the Southern Hemisphere. Meanwhile, changes in different physics schemes tend to impact different regions in the Southern Hemisphere. For instance, the role of CDNC is more substantial over the SO close to the Antarctic land, whereas the new trigger is more critical for the SO near mid-latitudes. The WBF rescaling, on the other hand, is influential on liquid and total clouds over the Antarctic land.

6. Summary and Discussion

In this study, we evaluate simulated cloud phase from EAMv2 and EAMv1 against CALIPSO-GOCCP observations. EAMv2 simulated cloud phase is compared with that predicted from EAMv1 to understand the model behavior change due to updated physics schemes and model tuning during the EAMv2 development. The focus of the analysis is on clouds simulated at high latitudes. In general, EAMv2 simulated total cloud cover over the Arctic region is still overestimated compared to CALIPSO-GOCCP, like EAMv1. The overly predicted low-level supercooled liquid phase clouds near the surface primarily contribute to the positive bias in total clouds. The maximum cloud bias in liquid clouds is found in boreal winter, but the positive bias is also found all year round. Although EAMv2 simulated liquid clouds insignificantly differ from EAMv1, ice phase clouds are largely improved in EAMv2 over the Arctic. Not only has the negative bias in ice clouds identified in EAMv1 been reduced, but also the overestimated ice clouds over the Norwegian Sea and Barents Sea become comparable to CALIPSO-GOCCP. Over the SO, compensating errors from liquid and ice phases and from different seasons result in comparable annual mean total cloud covers in EAMv2 against observations. Compared to EAMv1, positive biases in ice cloud cover are decreased in all seasons in EAMv2, but positive biases in liquid cloud cover are enhanced. Over Antarctica, the underestimation of ice cloud cover dominates the bias of total cloud in EAMv2, which is the same as EAMv1.

The primary reason for the improved cloud phase in EAMv2 is identified through a set of sensitivity experiments. First, it is found that the suppression of convection initiation due to the use of the new dCAPE_ULL trigger significantly improves the simulated cloud phase over the open ocean (e.g., Norwegian Sea, Barents Sea, and SO) in both hemispheres. Interestingly, the impact of modified trigger in the ZM scheme is crucial not only for tropical and subtropical precipitation (Golaz et al., 2022; Xie et al., 2019) but also for high latitude stratiform cloud phase. Note that the reduced initiation frequency of ZM scheme over high-latitude regions is physically reasonable because deep convective conditions are less likely to be satisfied at high latitudes than mid-latitudes and tropics in nature.

Second, it is found that changing the scaling factor of the WBF process from 0.1 to 0.7 substantially reduces the underestimation of cloud ice in EAMv1 simulated mixed-phase clouds. Increased ice and decreased liquid clouds are significant within the mixed-phase cloud temperature range (0 – -40°C) in both hemispheres, but excessive ice clouds are also produced due to this tuning parameter in EAMv2. This suggests that a more accurate and physically based representation of the WBF process in mixed-phase clouds is needed in the future model development. For example, early studies have illustrated that the occurrence of WBF process is expected only under limited conditions in mixed-phase clouds. Only when the local water vapor pressure exceeds the saturation vapor pressure with respect to ice and remains lower than saturation vapor pressure with respect to liquid, can the WBF process occur (Korolev, 2007; Fan et al., 2011). Accurately representing the onset of WBF process based on cloud dynamics that alters the local saturation can be helpful. Meanwhile, the WBF process is affected by the mixing states between liquid and ice in mixed-phase clouds (Korolev et al., 2017). The heterogeneous mixture of cloud hydrometeors can reduce the contact volume of liquid and ice, which further affects the WBF process strength (Tan & Storelvmo, 2016; M. Zhang et al., 2019). Properly representing the heterogeneity in the mixture between liquid and ice is also important for the WBF process.

Finally, we find that introducing a minimum CDNC in cloud microphysics is also responsible for increased liquid cloud cover in both hemispheres. This is because of the stronger liquid water production in relatively clean conditions due to the removal of unrealistic small CDNC by setting the low limit in EAMv2. We should note that other updates in cloud microphysics schemes and model tuning as discussed in Golaz et al. (2022) can also influence the simulated cloud phase. For example, recalibrated tuning parameters in deep convection largely increase ice clouds over the Arctic, but the impact is negligible for the SO and Antarctica. Moreover, the impacts of modified tuning parameters in CLUBB and microphysics scheme are also examined (not shown). It is found that the recalibrated tunings in CLUBB and microphysics, as well as the modified treatment of surface gustiness tend to slightly increase liquid clouds over the SO (minimal change in the Arctic), but their impacts are not as large as what are shown in the four sensitivity experiments.

Note that the cloud evaluation purely based on the CALIPSO-GOCCP observation is influenced by the instrument limitation of CALIOP lidar. The attenuation of lidar signal due to liquid layers may limit the ability of the CALIPSO satellite to detect low-level mixed-phase clouds that are commonly observed at high latitudes. Therefore, an ongoing separate work utilizing the DOE ARM program's ground-based remote sensing retrievals to evaluate modeled mixed-phase cloud properties will complement our current study. The combined ground-based radar and lidar measurements have provided reliable cloud detections and cloud property retrievals of high-latitude mixed-phase clouds (Shupe et al., 2008, 2011; D. Zhang et al., 2019). Model evaluation against the ARM ground-based measurements will be presented in a separate study.

To conclude, EAMv2 has improved the simulated cloud climatology compared to EAMv1. The better cloud ice phase prediction by EAMv2 should have an important impact on the future climate simulation. However, the remaining cloud biases, such as the overestimation of liquid clouds in the entire Arctic and the SO, as well as the underestimation of ice clouds over the Antarctic land, require further improvements in the future model development. Detailed cloud regime-based analysis is also necessary to further understand model cloud biases.

Acknowledgment: This research was supported as part of the Energy Exascale Earth System Model (E3SM) project, funded by the U.S. Department of Energy, Office of Science, Office of Biological and Environmental Research. Work at LLNL was performed under the auspices of the U.S. DOE by Lawrence Livermore National Laboratory under contract No. DE-AC52-07NA27344. Xiaohong Liu acknowledges the funding support by the DOE Atmospheric System Research (ASR) Program (grant DE-SC0020510). This research used resources of the National Energy Research Scientific Computing Center (NERSC), a U.S. Department of Energy Office of Science User Facility located at Lawrence Berkeley National Laboratory, operated under Contract No.DE-AC02-05CH11231.

Data Availability Statement: The model codes may be accessed at https://github.com/E3SM-Project/E3SM. The model data used in this study can be accessible at https://portal.nersc.gov/archive/home/m/mengz/www/Zhang-E3SMv2-MixedPhaseClouds. The CALIPSO-GOCCP observational data is available online at https://climserv.ipsl.polytechnique.fr/cfmip-obs/Calipso_goccp.html.

References

Adhikari, L., Wang, Z., & Deng, M. (2012). Seasonal variations of Antarctic clouds observed by CloudSat and CALIPSO satellites, *Journal of Geophysical Research: Atmospheres*, 117, D04202. https://doi.org/10.1029/2011JD016719

Bey, I., Jacob, D. J., Yantosca, R. M., Logan, J. A., Field, B. D., Fiore, A. M., et al. (2001). Global modeling of tropospheric chemistry with assimilated meteorology: Model description and evaluation, *Journal of Geophysical Research: Atmospheres*, 106(D19), 23073–23095. https://doi.org/10.1029/2001JD000807

Bjordal, J., Storelvmo, T., Alterskjær, K. & Carlsen, T. (2020). Equilibrium climate sensitivity above 5 °C plausible due to state-dependent cloud feedback, *Nature Geoscience*, 13, 718–721. https://doi.org/10.1038/s41561-020-00649-1

Bodas-Salcedo, A., Hill, P. G., Furtado, K., Williams, K. D., Field, P. R., Manners, J. C., Hyder, P., & Kato, S. (2016). Large Contribution of Supercooled Liquid Clouds to the Solar Radiation Budget of the Southern Ocean, *Journal of Climate*, 29(11), 4213–4228. https://doi.org/10.1175/JCLI-D-15-0564.1

Bodas-Salcedo, A., Webb, M. J., Bony, S., Chepfer, H., Dufresne, J., Klein, S. A., et al. (2011). COSP: Satellite simulation software for model assessment, *Bulletin of the American Meteorological Society*, 92(8), 1023–1043. https://doi.org/10.1175/2011BAMS2856.1

Bodas-Salcedo, A., Mulcahy, J. P., Andrews, T., Williams, K. D., Ringer, M. A., Field, P. R., & Elsaesser, G. S. (2019). Strong dependence of atmospheric feedbacks on mixed-phase microphysics and aerosol-cloud interactions in HadGEM3. *Journal of Advances in Modeling Earth Systems*, 11, 1735–1758. https://doi.org/10.1029/2019MS001688

Bogenschutz, P. A., Gettelman, A., Morrison, H., Larson, V. E., Craig, C., & Schanen, D. P. (2013). Higher-order turbulence closure and its impact on climate simulations in the Community Atmosphere Model. *Journal of Climate*, 26(23), 9655–9676. https://doi.org/10.1175/JCLI-D-13-00075.1

Cesana, G., & Chepfer, H. (2012). How well do climate models simulate cloud vertical structure? A comparison between CALIPSO-GOCCP satellite observations and CMIP5 models, *Geophysical Research Letters*, 39, L20803. https://doi.org/10.1029/2012GL053153

Cesana, G., & Chepfer, H. (2013). Evaluation of the cloud thermodynamic phase in a climate model using CALIPSO-GOCCP. *Journal of Geophysical Research: Atmosphere*, 118, 7922–7937. https://doi.org/10.1002/jgrd.50376

Cesana, G., Kay, J. E., Chepfer, H., English, J. M., & de Boer, G. (2012). Ubiquitous low-level liquid-containing Arctic clouds: New observations and climate model constraints from CALIPSO-GOCCP, *Geophysical Research Letters*, 39, L20804. https://doi.org/10.1029/2012GL053385

Chepfer, H., Bony, S., Winker, D., Chiriaco, M., Dufresne, J.-L., & Sèze, G. (2008). Use of CALIPSO lidar observations to evaluate the cloudiness simulated by a climate model, *Geophysical Research Letters*, 35, L15704. https://doi.org/10.1029/2008GL034207

Chepfer, H., Bony, S., Winker, D., Cesana, G., Dufresne, J. L., Minnis, P., Stubenrauch, C. J., & Zeng, S. (2010). The GCM-Oriented CALIPSO Cloud Product (CALIPSO-GOCCP), *Journal of Geophysical Research: Atmospheres*, 115, D00H16. https://doi.org/10.1029/2009JD012251

Cox, C. J., Turner, D. D., Rowe, P. M., Shupe, M. D., & Walden, V. P. (2014). Cloud Microphysical Properties Retrieved from Downwelling Infrared Radiance Measurements Made at Eureka, Nunavut, Canada (2006–09), *Journal of Applied Meteorology and Climatology*, 53(3), 772–791. https://doi.org/10.1175/JAMC-D-13-0113.1

Curry, J. A., & Ebert, E. E. (1992). Annual Cycle of Radiation Fluxes over the Arctic Ocean: Sensitivity to Cloud Optical Properties, *Journal of Climate*, 5(11), 1267–1280. https://doi.org/10.1175/1520-0442(1992)005<1267:ACORFO>2.0.CO;2

Curry, J. A., Schramm, J. L., Rossow, W. B., & Randall, D. (1996). Overview of Arctic Cloud and Radiation Characteristics, *Journal of Climate*, 9(8), 1731–1764. https://doi.org/10.1175/1520-0442(1996)009<1731:OOACAR>2.0.CO;2

de Boer, G., Eloranta, E. W., & Shupe, M. D. (2009). Arctic Mixed-Phase Stratiform Cloud Properties from Multiple Years of Surface-Based Measurements at Two High-Latitude Locations, *Journal of the Atmospheric Sciences*, 66(9), 2874–2887. https://doi.org/10.1175/2009JAS3029.1

Dubovik, O., Smirnov, A., Holben, B. N., King, M. D., Kaufman, Y. J., Eck, T. F., & Slutsker, I. (2000). Accuracy assessments of aerosol optical properties retrieved from aerosol robotic network (AERONET) sun and sky radiance measurements. *Journal of Geophysical Research: Atmospheres*, 105 (D8). 9791–9806. https://doi.org/10.1029/2000jd900040

English, J. M., Kay, J. E., Gettelman, A., Liu, X., Wang, Y., Zhang, Y., & Chepfer, H. (2014). Contributions of Clouds, Surface Albedos, and Mixed-Phase Ice Nucleation Schemes to Arctic Radiation Biases in CAM5, *Journal of Climate*, 27(13), 5174–5197. https://doi.org/10.1175/JCLI-D-13-00608.1

Fan, J., Ghan, S., Ovchinnikov, M., Liu, X., Rasch, P. J., & Korolev, A. (2011). Representation of Arctic mixed-phase clouds and the Wegener-Bergeron-Findeisen process in climate models: Perspectives from a cloud-resolving study. *Journal of Geophysical Research: Atmospheres*, 116, D00T07. https://doi.org/10.1029/2010JD015375

Field, P. R., & Heymsfield, A. J. (2015). Importance of snow to global precipitation, *Geophysical Research Letters*, 42, 9512–9520. https://doi.org/10.1002/2015GL065497

Feng, Y., Wang, H., Rasch, P. J., Zhang, K., Lin, W., Tang, Q., et al. (2022). Global dust cycle and direct radiative effect in E3SM version 1: Impact of increasing model resolution. *Earth and Space Science Open Archive*, 50. https://doi.org/148710.1002/essoar.10510950.1

Forbes, R. M., & Ahlgrimm, M. (2014). On the Representation of High-Latitude Boundary Layer Mixed-Phase Cloud in the ECMWF Global Model, *Monthly Weather Review*, 142(9), 3425–3445. https://doi.org/10.1175/MWR-D-13-00325.1

Gettelman, A., Hannay, C., Bacmeister, J. T., Neale, R. B., Pendergrass, A. G., Danabasoglu, G., et al. (2019). High climate sensitivity in the Community Earth System Model Version 2 (CESM2). *Geophysical Research Letters*, 46, 8329–8337. https://doi.org/10.1029/2019GL083978

Gettelman, A., & Morrison, H. (2014). Advanced two-moment bulk microphysics for global models. Part I: Off-line tests and comparison with other schemes. *Journal of Climate*, 28(3), 1268–1287. https://doi.org/10.1175/JCLI-D-14-00102.1

Gettelman, A., Morrison, H., Santos, S., Bogenschutz, P., & Caldwell, P. M. (2015). Advanced two-moment bulk microphysics for global models. Part II: Global model solutions and aerosol–cloud interactions. *Journal of Climate*, 28(3), 1288–1307. https://doi.org/10.1175/JCLI-D-14-00103.1

Golaz, J.-C., Caldwell, P. M., Van Roekel, L. P., Petersen, M. R., Tang, Q., Wolfe, J. D., et al. (2019). The DOE E3SM coupled model version 1: Overview and evaluation at standard resolution. *Journal of Advances in Modeling Earth Systems*, 11, 2089–2129. https://doi.org/10.1029/2018MS001603

Golaz, J.-C., Larson, V. E., & Cotton, W. R. (2002). A PDF-based model for boundary layer clouds. Part I: Method and model description. *Journal of the Atmospheric Sciences*, 59(24), 3540–3551. https://doi.org/10.1175/1520-0469(2002)059<3540:APBMFB>2.0.CO;2

Golaz, J.-C., Van Roekel, P. L., Zheng, X., Roberts, A., Wolfe, D. J., Lin, W., et al. (2022). The DOE E3SM Model Version 2: Overview of the physical model. *Earth and Space Science Open Archive*. https://doi.org/10.1002/essoar.10511174.1

Hannah, W. M., Bradley, A. M., Guba, O., Tang, Q., Golaz, J.-C., & Wolfe, J. (2021). Separating physics and dynamics grids for improved computational efficiency in spectral element earth system models. *Journal of Advances in Modeling Earth Systems*, 13, e2020MS002419. https://doi.org/10.1029/2020MS002419

Harrop, B. E., Ma, P.-L., Rasch, P. J., Neale, R. B., & Hannay, C. (2018). The role of convective gustiness in reducing seasonal precipitation biases in the tropical west pacific. *Journal of Advances in Modeling Earth Systems*, 10 (4), 961–970. https://doi.org/10.1002/2017MS001157

Heymsfield, A. J., Schmitt, C., Chen, C., Bansemer, A., Gettelman, A., Field, P. R., & Liu, C. (2020). Contributions of the Liquid and Ice Phases to Global Surface Precipitation: Observations and Global Climate Modeling, *Journal of the Atmospheric Sciences*, 77(8), 2629–2648. https://doi.org/10.1175/JAS-D-19-0352.1

Hoose, C., Kristjánsson, J. E., Chen, J. P., & Hazra, A. (2010). A classical-theory-based parameterization of heterogeneous ice nucleation by mineral dust, soot, and biological particles in a global climate model. *Journal of the Atmospheric Sciences*, 67(8), 2483–2503. https://doi.org/10.1175/2010JAS3425.1

Hsu, J., & Prather, M. J. (2009). Stratospheric variability and tropospheric ozone. *Journal of Geophysical Research: Atmospheres*, 114, D06102. https://doi.org/10.1029/2008JD010942

Hu, Y., Rodier, S., Xu, K., Sun, W., Huang, J., Lin, B., Zhai, P., & Josset, D. (2010). Occurrence, liquid water content, and fraction of supercooled water clouds from combined CALIOP/IIR/MODIS measurements, *Journal of Geophysical Research: Atmospheres*, 115, D00H34. https://doi.org/10.1029/2009JD012384

Iacono, M. J., Delamere, J. S., Mlawer, E. J., Shephard, M. W., Clough, S. A., & Collins, W. D. (2008). Radiative forcing by long-lived greenhouse gases: Calculations with the AER radiative transfer models. *Journal of Geophysical Research: Atmospheres*, 113, D13103. https://doi.org/10.1029/2008JD009944

Intrieri, J. M., Shupe, M. D., Uttal, T., & McCarty, B. J. (2002). An annual cycle of Arctic cloud characteristics observed by radar and lidar at SHEBA, *Journal of Geophysical Research: Atmospheres*, 107(C10). https://doi.org/10.1029/2000JC000423

Kay, J. E., Bourdages, L., Miller, N. B., Morrison, A., Yettella, V., Chepfer, H., & Eaton, B. (2016). Evaluating and improving cloud phase in the Community Atmosphere Model version 5 using spaceborne lidar observations, *Journal of Geophysical Research: Atmospheres*, 121, 4162–4176. https://doi.org/10.1002/2015JD024699

Kay, J. E., Hillman, B. R., Klein, S. A., Zhang, Y., Medeiros, B., Pincus, R., et al. (2012). Exposing Global Cloud Biases in the Community Atmosphere Model (CAM) Using Satellite Observations and Their Corresponding Instrument Simulators, *Journal of Climate*, 25(15), 5190–5207. https://doi.org/10.1175/JCLI-D-11-00469.1

Korolev, A. (2007). Limitations of the Wegener-Bergeron-Findeisen mechanism in the evolution of mixed-phase clouds. *Journal of the Atmospheric Sciences*, 64, 3372-3375. https://doi.org/10.1175/JAS4035.1

Korolev, A., McFarquhar, G., Field, P. R., Franklin, C., Lawson, P., Wang, Z., et al. (2017). Mixed-Phase Clouds: Progress and Challenges. *Meteorological Monographs*. 58, 5.1-5.50. https://doi.org/10.1175/AMSMONOGRAPHS-D-17-0001.1

Larson, V. E. (2017). CLUBB-SILHS: A parameterization of subgrid variability in the atmosphere. arXiv preprint arXiv:1711.03675v2.

Larson, V. E., & Golaz, J.-C. (2005). Using probability density functions to derive consistent closure relationships among higher-order moments. *Monthly Weather Review*, 133(4), 1023–1042. https://doi.org/10.1175/MWR2902.1

Liu, X., Easter, R. C., Ghan, S. J., Zaveri, R., Rasch, P., Shi, X., et al. (2012). Toward a minimal representation of aerosols in climate models: description and evaluation in the Community Atmosphere Model CAM5, *Geoscientific Model Development*, 5, 709–739. https://doi.org/10.5194/gmd-5-709-2012

Liu, X., Ma, P.-L., Wang, H., Tilmes, S., Singh, B., Easter, R. C., et al. (2016). Description and evaluation of a new four-mode version of the Modal Aerosol Module (MAM4) within version 5.3 of the Community Atmosphere Model. *Geoscientific Model Development*, 9(2), 505–522. https://doi.org/10.5194/gmd-9-505-2016

Lohmann, U. & Neubauer, D. (2018). The importance of mixed-phase and ice clouds for climate sensitivity in the global aerosol–climate model ECHAM6-HAM2, *Atmospheric Chemistry and Physics*, 18, 8807–8828. https://doi.org/10.5194/acp-18-8807-2018

Lubin, D., Zhang, D., Silber, I., Scott, R. C., Kalogeras, P., Battaglia, A., et al. (2020). AWARE: The Atmospheric Radiation Measurement (ARM) West Antarctic Radiation Experiment, *Bulletin of the American Meteorological Society*, 101(7), E1069-E1091. https://doi.org/10.1175/BAMS-D-18-0278.1

Ma, P.-L., Harrop, B. E., Larson, V. E., Neale, R., Gettelman, A., Morrison, H., et al. (2021). Better calibration of cloud parameterizations and subgrid effects increases the fidelity of E3SM

Atmosphere Model version 1, *Geoscientific Model Development Discussion.* https://doi.org/10.5194/gmd-2021-298

McCoy, D. T., Hartmann, D. L., Zelinka, M. D., Ceppi, P., & Grosvenor, D. P. (2015). Mixed-phase cloud physics and Southern Ocean cloud feedback in climate models, *Journal of Geophysical Research: Atmospheres*, 120, 9539–9554, https://doi.org/10.1002/2015JD023603

McCoy, D. T., Tan, I., Hartmann, D. L., Zelinka, M. D., & Storelvmo, T. (2016). On the relationships among cloud cover, mixed-phase partitioning, and planetary albedo in GCMs, *Journal of Advances in Modeling Earth Systems*, 8, 650–668. https://doi.org/10.1002/2015MS000589

McFarquhar, G. M., Bretherton, C. S., Marchand, R., Protat, A., DeMott, P. J., Alexander, S. P., et al. (2021). Observations of Clouds, Aerosols, Precipitation, and Surface Radiation over the Southern Ocean: An Overview of CAPRICORN, MARCUS, MICRE, and SOCRATES, *Bulletin of the American Meteorological Society*, 102(4), E894–E928. https://doi.org/10.1175/BAMS-D-20-0132.1

Mlawer, E. J., Taubman, S. J., Brown, P. D., Iacono, M. J., & Clough, S. A. (1997). Radiative transfer for inhomogeneous atmospheres: RRTM, a validated correlated-k model for the longwave. *Journal of Geophysical Research: Atmospheres*, 102(D14), 16,663–16,682. https://doi.org/ 10.1029/97JD00237

Morrison, H., de Boer, G., Feingold, G., Harrington, J., Shupe, M. D. & Sulia, K. (2012). Resilience of persistent Arctic mixed-phase clouds. *Nature Geoscience*, 5, 11–17. https://doi.org/10.1038/ngeo1332

Morrison, H., van Lier-Walqui, M., Fridlind, A. M., Grabowski, W. W., Harrington, J. Y., Hoose, C., et al. (2020). Confronting the challenge of modeling cloud and precipitation microphysics. *Journal of Advances in Modeling Earth Systems*, 12, e2019MS001689. https://doi.org/10.1029/2019MS001689

Mülmenstädt, J., Sourdeval, O., Delanoë, J., & Quaas, J. (2015). Frequency of occurrence of rain from liquid-, mixed-, and ice-phase clouds derived from A-Train satellite retrievals. *Geophysical Research Letters*, 42, 6502–6509. https://doi.org/10.1002/2015GL064604

Murray, B. J., Carslaw, K. S., & Field, P. R. (2021). Opinion: Cloud-phase climate feedback and the importance of ice-nucleating particles, *Atmospheric Chemistry and Physics*, 21, 665–679. https://doi.org/10.5194/acp-21-665-2021

Rasch, P. J., Xie, S., Ma, P.-L., Lin, W., Wang, H., Tang, Q., et al. (2019). An overview of the atmospheric component of the Energy Exascale Earth System Model. *Journal of Advances in Modeling Earth Systems*, 11, 2377–2411. https://doi.org/10.1029/2019MS001629

Redelsperger, J., Guichard, F., & Mondon, S. (2000). A Parameterization of Mesoscale Enhancement of Surface Fluxes for Large-Scale Models, *Journal of Climate*, 13(2), 402–421. https://doi.org/10.1175/1520-0442(2000)013<0402:APOMEO>2.0.CO;2

Sedlar, J., Shupe, M. D., & Tjernström, M. (2012). On the Relationship between Thermodynamic Structure and Cloud Top, and Its Climate Significance in the Arctic, *Journal of Climate*, 25(7), 2374–2393. https://doi.org/10.1175/JCLI-D-11-00186.1

Shupe, M. D. (2011). Clouds at Arctic Atmospheric Observatories. Part II: Thermodynamic Phase Characteristics, *Journal of Applied Meteorology and Climatology*, 50(3), 645–661. https://doi.org/10.1175/2010JAMC2468.1

Shupe, M. D., Matrosov, S. Y., & Uttal, T. (2006). Arctic Mixed-Phase Cloud Properties Derived from Surface-Based Sensors at SHEBA, *Journal of the Atmospheric Sciences*, 63(2), 697–711. https://doi.org/10.1175/JAS3659.1

Shupe, M. D., Walden, V. P., Eloranta, E., Uttal, T., Campbell, J. R., Starkweather, S. M., & Shiobara, M. (2011). Clouds at Arctic Atmospheric Observatories. Part I: Occurrence and Macrophysical Properties, *Journal of Applied Meteorology and Climatology*, 50(3), 626–644. https://doi.org/10.1175/2010JAMC2467.1

Shupe, M. D., & Intrieri, J. M. (2004). Cloud Radiative Forcing of the Arctic Surface: The Influence of Cloud Properties, Surface Albedo, and Solar Zenith Angle, *Journal of Climate*, 17(3), 616–628. https://doi.org/10.1175/1520-0442(2004)017<0616:CRFOTA>2.0.CO;2

Sun, Z. & Shine, K. P. (1994). Studies of the radiative properties of ice and mixed-phase clouds. *Quarterly Journal of the Royal Meteorological Society*, 120, 111–137. https://doi.org/10.1002/qj.49712051508

Swales, D. J., Pincus, R., & Bodas-Salcedo, A. (2018). The Cloud Feedback Model Intercomparison Project Observational Simulator Package: Version 2, *Geoscientific Model Development*, 11, 77–81. https://doi.org/10.5194/gmd-11-77-2018

Tan, I., & Storelvmo, T. (2016). Sensitivity study on the influence of cloud microphysical parameters on mixed-phase cloud thermodynamic phase partitioning in CAM5. *Journal of the Atmospheric Sciences*, 73, 709-728. https://doi.org/10.1175/JAS-D-15-0152.1

Tan, I., Storelvmo, T., & Zelinka, M. D. (2016). Observational constraints on mixed-phase clouds imply higher climate sensitivity. *Science*, 352, 224-227. https://doi.org/10.1126/science.aad5300

Tang, Q., Prather, M. J., Hsu, J., Ruiz, D. J., Cameron-Smith, P. J., Xie, S., & Golaz, J.-C. (2021). Evaluation of the interactive stratospheric ozone (O3v2) module in the E3SM version 1 Earth system model, *Geoscientific Model Development*, 14, 1219–1236. https://doi.org/10.5194/gmd-14-1219-2021

Tsushima, Y., Emori, S., Ogura, T., Kimoto, M., Webb, M. J., Williams, K. D. et al. (2006). Importance of the mixed-phase cloud distribution in the control climate for assessing the response of clouds to carbon dioxide increase: a multi-model study. *Climate Dynamics*, 27, 113–126. https://doi.org/10.1007/s00382-006-0127-7

Wang, H., Easter, R. C., Zhang, R., Ma, P.-L., Singh, B., Zhang, K., et al. (2020). Aerosols in the E3SM Version 1: New developments and their impacts on radiative forcing. *Journal of Advances in Modeling Earth Systems*, 12, e2019MS001851. https://doi.org/10.1029/2019MS001851

Wang, Y., Liu, X., Hoose, C., & Wang, B. (2014). Different contact angle distributions for heterogeneous ice nucleation in the Community Atmospheric Model version 5. *Atmospheric Chemistry and Physics*, 14, 10411–10430. https://doi.org/10.5194/acp-14-10411-2014

Wang, Y.-C., Pan, H.-L., & Hsu, H.-H. (2015). Impacts of the triggering function of cumulus parameterization on warm-season diurnal rainfall cycles at the Atmospheric Radiation Measurement Southern Great Plains Site. *Journal of Geophysical Research: Atmospheres*, 120, 10681–10702. https://doi.org/10.1002/2015JD023337

Wang, Y.-C., Xie, S., Tang, S., & Lin, W. (2020). Evaluation of an improved convective triggering function: Observational evidence and SCM tests. *Journal of Geophysical Research: Atmospheres*, 125, e2019JD031651. https://doi.org/10.1029/e2019JD031651

Winker, D. M., Hunt, W. H., & McGill, M. J. (2007). Initial performance assessment of CALIOP, *Geophysical Research Letters*, 34, L19803. https://doi.org/10.1029/2007GL030135

Winker, D. M., Vaughan, M. A., Omar, A., Hu, Y., Powell, K. A., Liu, Z., Hunt, W. H., & Young, S. A. (2009). Overview of the CALIPSO Mission and CALIOP Data Processing Algorithms, *Journal of Atmospheric and Oceanic Technology*, 26(11), 2310–2323. https://doi.org/10.1175/2009JTECHA1281.1

Xie, S., Boyle, J., Klein, S. A., Liu, X., & Ghan, S. (2008). Simulations of Arctic mixed-phase clouds in forecasts with CAM3 and AM2 for MPACE. *Journal of Geophysical Research: Atmospheres*, 113, D04211. https://doi.org/10.1029/2007JD009225

Xie, S., Lin, W., Rasch, P. J., Ma, P.-L., Neale, R., Larson, V. E., et al. (2018). Understanding cloud and convective characteristics in version 1 of the E3SM atmosphere model. *Journal of Advances in Modeling Earth Systems*, 10, 2618–2644. https://doi.org/10.1029/2018MS001350

Xie, S., Liu, X., Zhao, C., & Zhang, Y. (2013). Sensitivity of CAM5-Simulated Arctic Clouds and Radiation to Ice Nucleation Parameterization. *Journal of Climate*, 26(16), 5981–5999. https://doi.org/10.1175/JCLI-D-12-00517.1

Xie, S., Wang, Y.-C., Lin, W., Ma, H.-Y., Tang, Q., Tang, S., et al. (2019). Improved diurnal cycle of precipitation in E3SM with a revised convective triggering function. *Journal of Advances in Modeling Earth Systems*, 11. https://doi.org/10.1029/2019MS001702

Xie, S., & Zhang, M. (2000). Impact of the convection triggering function on single-column model simulations. *Journal of Geophysical Research: Atmospheres*, 105(D11), 14983–14996. https://doi.org/10.1029/2000JD900170

Zelinka, M. D., Myers, T. A., McCoy, D. T., Po-Chedley, S., Caldwell, P. M., Ceppi, P., et al. (2020). Causes of higher climate sensitivity in CMIP6 models. *Geophysical Research Letters*, 47, e2019GL085782. https://doi.org/10.1029/2019GL085782

Zhang, D., Wang, Z., Kollias, P., Vogelmann, A. M., Yang, K., & Luo, T. (2018). Ice particle production in mid-level stratiform mixed-phase clouds observed with collocated A-Train measurements. *Atmospheric Chemistry and Physics*, 18, 4317–4327. https://doi.org/10.5194/acp-18-4317-2018

Zhang, D., Wang, Z. & Liu, D. (2010). A global view of midlevel liquid-layer topped stratiform cloud distribution and phase partition from CALIPSO and CloudSat measurements, *Journal of Geophysical Research: Atmospheres*, 115, D00H13. https://doi.org/10.1029/2009JD012143

Zhang, D., Vogelmann, A., Kollias, P., Luke, E., Yang, F., Lubin, D., & Wang, Z. (2019). Comparison of Antarctic and Arctic single-layer stratiform mixed-phase cloud properties using ground-based remote sensing measurements. *Journal of Geophysical Research: Atmospheres*, 124. https://doi.org/10.1029/2019JD030673

Zhang, G. J., & McFarlane, N. A. (1995). Sensitivity of climate simulations to the parameterization of cumulus convection in the Canadian climate centre general circulation model. *Atmosphere-Ocean*, 33(3), 407–446. https://doi.org/10.1080/07055900.1995.9649539

Zhang, M., Liu, X., Diao, M., D'Alessandro, J. J., Wang, Y., Wu, C., et al. (2019). Impacts of representing heterogeneous distribution of cloud liquid and Ice on phase partitioning of Arctic mixed-phase clouds. *Journal of Geophysical Research: Atmospheres*, 124, 13071–13090. https://doi.org/10.1029/2019JD030502

Zhang, M., Xie, S., Liu, X., Lin, W., Zhang, K., Ma, H.-Y., et al. (2020). Toward understanding the simulated phase partitioning of arctic single-layer mixed-phase clouds in E3SM. *Earth and Space Science*, 7, e2020EA001125. https://doi.org/10.1029/2020EA001125

Zhang, M., & Bretherton, C. (2008). Mechanisms of Low Cloud–Climate Feedback in Idealized Single-Column Simulations with the Community Atmospheric Model, Version 3 (CAM3), *Journal of Climate*, 21(18), 4859–4878. https://doi.org/10.1175/2008JCLI2237.1

Zhang, M., Bretherton, C. S., Blossey, P. N., Austin, P. H., Bacmeister, J. T., Bony, S., et al. (2013). CGILS: Results from the first phase of an international project to understand the physical mechanisms of low cloud feedbacks in single column models, *Journal of Advances in Modeling Earth Systems*, 5, 826–842. https://doi.org/10.1002/2013MS000246

Zhang, M. H., Lin, W. Y., Klein, S. A., Bacmeister, J. T., Bony, S., Cederwall, R. T., et al. (2005). Comparing clouds and their seasonal variations in 10 atmospheric general circulation models with satellite measurements, *Journal of Geophysical Research: Atmospheres*, 110, D15S02. https://doi.org/10.1029/2004JD005021

Zhang, Y., Klein, S. A., Boyle, J., & Mace, G. G. (2010). Evaluation of tropical cloud and precipitation statistics of Community Atmosphere Model version 3 using CloudSat and CALIPSO data, *Journal of Geophysical Research: Atmospheres*, 115, D12205. https://doi.org/10.1029/2009JD012006

Zhang, Y., Xie, S., Lin, W., Klein, S. A., Zelinka, M., Ma, P.-L., et al. (2019). Evaluation of clouds in version 1 of the E3SM atmosphere model with satellite simulators. *Journal of Advances in Modeling Earth Systems*, 11. https://doi.org/10.1029/2018MS001562